Bibliography

[1] D. Griffiths, *Introduction to Elementary Particles*, Wiley Publishers, New York, 1987.

[2] Particle Data Group, *European Physical Journal* **C3** (1998) 1.

[3] M. Gell-Mann, *Phys. Lett.* **8** (1964) 214.

[4] G. Zweig, CERN report 8182/TH (unpublished) 1964; CERN Report 8419/TH (unpublished) 1964.

[5] M. Gell-Mann *Phys. Rev. Lett.* **12** (1964) 155.

[6] O. W. Greenberg, *Phys. Rev. Lett.* **13** (1964) 20.

[7] M. Gell-Mann, *Acta Physica Austiraca Suppl.* **IX** (1972) 733

[8] D. Thompson *et al.* , *Phys. Rev. Lett.* **79** (1997) 1630, G.S. Adams *et al.* , *Phys. Rev. Lett.* **81** (1998) 5761.

[9] A. Abele *et al.* , *Phys. Lett.* **B423** (1998) 175.

[10] B. J. Bjorken and S. L. Glashow, *Phys. Lett.* **11** (1964) 255.

[11] S. L. Glashow, J. Iliopoulos and L. Maiani, *Phys. Rev.* **D2** (1970) 1285.

[12] T. Appelquist and H. D. Politzer, *Phys. Rev. Lett.* **34** (1975) 43.

[13] E. Eichten, *et al.* , *Phys. Rev.* **D17** (1980) 3090; *ibid.* **21** (1980) 313(E); *ibid.* **21** (1980) 203.

[14] J. L. Richardson, *Phys. Lett.* **82B** (1979) 272.

[15] C. Quigg and J. L. Rosner, *Phys. Rep.* **56** (1979) 167.

[16] A nice collection of papers relating to the development of QED is found in "Selected Papers on Quantum Electrodynamics", ed. by J. Schwinger, (New York: Dover, 1958).

[17] B. J. Bjorken and S. D. Drell, *Relativistic Quantum Mechanics*, McGraw-Hill Book Company, New York, 1965, p. (point to Appendix).

[18] J. A. Wheeler, *Ann. NY Acad. Sci.***48** (1946) 219.

[19] C. N. Yang, *Phys. Rev.* **77** (1950) 242.

[20] I. B. Khriplovich and A. S. Yelkhovsky, *Phys. Lett.* **B246** (1990) 520.

[21] A. H. Al-Ramadhan and D. W. Gidley, *Phys. Rev. Lett.* **72** (1994) 1632.

[22] R. Van Royen and V. F. Weisskopf, *Nuovo Cim.* **A50** (1967) 617.

[23] W. Kwong *et al.* , *Phys. Rev.* **D37** (1988) 3210.

[24] J. J. Aubert *et al.* , *Phys. Rev. Lett.* **33** (1974) 1404.

[25] J.-E. Augustin *et al.* , *Phys. Rev. Lett.* **33** (1974) 1406.

[26] Very unusual proposals for the explanation of the J/ψ observation were offered by prominent physicists such as J. Schwinger, *Phys. Rev. Lett.* **34** (1974) 37, A. S. and M. Goldhaber, *Phys. Rev. Lett.* **34** (1974) 36 and H. T. Nieh, T. T. Wu and C. N. Yang, *Phys. Rev. Lett.* **34** (1974) 49.

[27] The parameters of the Antiproton Accumulator operation may be found in, among others, J. Peoples, *IEEE Trans. on Nucl. Sci.* **NS-30** (1983) 1970, and S. O'Day and F. M. Bieniosek, *Nucl. Instr. Meth.* **A343** (1994) 343. and

[28] A.V. Tollestrup and G. Dugan, "Elementary Stochastic Cooling," in *Physics of High Energy Particle Accelerators,* AIP Conference Proceedings No. 105, ed. by M. Month, pp. 954-1057.

[29] G. Dugan, CLEO Preprint CLNS-97-1532 (1997).

[30] D. Zholentz *et al.* , *Phys. Lett.* **96B** (1980) 214.

[31] D. Allspach *et al.* , *Nucl. Instr. Meth.* **A410** (1998) 195.

[32] G. Garzoglio, *priv. comm.*, November, 1998.

[33] J. Marques, Ph.D. dissertation, University of California at Irvine (unpublished), 1992.

[34] See, for example, D. Bettoni *et al.* , *IEEE Trans. on Nucl. Sci.* **44** (1997) 460, M. Ambrogiani *et al.* , "Results from the E835 Cylindrical Scintillating-Fiber

Tracker", *Proc. SCI-FI '97* or M. Ambrogiani *et al.* , "Performance Measurements of Histe-V VLPC Photon Detectors for E835 at FNAL", *op. cit.*

[35] C. Biino *et al.* , *Nucl. Instr. Meth.* **A271** (1988) 417.

[36] A. Buzzo *et al.* , *Nucl. Instr. Meth.* **A391** (1997) 443.

[37] C. Biino *et al.* , *Nucl. Instr. Meth.* **A317** (1992) 135.

[38] C. M. Ginsburg, Ph.D. dissertation, Northwestern University (unpublished), 1995.

[39] S. Bagnasco *et al.* , *submitted to Nucl. Instr. Meth. A.*

[40] K. E. Gollwitzer, Ph.D. dissertation, University of California at Irvine (unpublished), 1993.

[41] S. Trokenheim *et al.* , *Nucl. Instr. Meth.* **A355** (1995) 308.

[42] T. A. Armstrong *et al.* , *Phys. Lett.* **B385** (1996) 479.

[43] S. Trokenheim, Ph.D. dissertation, Northwestern University (unpublished), 1994.

[44] R. Ray *et al.* , *Nucl. Instr. Meth.* **A307** (1991) 254.

[45] S. Jin and J. L. Rosen, E835 Memo (January 1999), 'E835 Neutral Trigger'.

[46] L. Bartosek *et al.* , *Nucl. Instr. Meth.* **A301** (1991) 47.

[47] G. Stancari, E835 Internal Memo #369, 'Measurement of the Magnetic Form Factor of the Proton'.

[48] J. E. Fast, Ph.D. dissertation, University of California at Irvine (unpublished), 1992.

[49] M. Masuzawa, Ph.D. dissertation, Northwestern University (unpublished), 1994.

[50] T. A. Armstrong *et al.* ,*Phys. Rev.* **D52** (1995) 4839.

[51] T. A. Armstrong *et al.* , *Phys. Rev.* **D56** (1997) 2509.

[52] M. Ambrogiani, presentation on χ_J angular distributions at Torino E835 Meeting, Feb. 1998. The results of her study should be compared to the E760 paper on the χ_2 angular distribution: *Phys. Rev.* **D48** (1993) 3037.

[53] Z. P. Li, F. Close and T. Barnes, *Phys. Rev.* **D43** (1991) 2161.

[54] H. Hamasaki *et al.* , *Phys. Lett.* **B407** (1997) 185.

[55] M. Artuso *et al.* , *Phys. Rev.* **D50** (1994) 5484.

[56] P. Kroll *et al.* , *Phys. Lett.* **B316** (1993) 546.

[57] F. James and M. Roos, "MINUIT, Function Minimization and Error Analysis," CERN D506 (Long Writeup).

[58] Particle Data Group, *Phys. Rev.* **D49** (1994) 1.

[59] D. Bisello *et al.* , *Phys. Lett.* **B350** (1991) 1.

[60] J. Z. Bai *et al.* , *Phys. Rev. Lett.* **65** (1990) 1311.

[61] C. Baglin *et al.* , *Phys. Lett.* **187B** (1987) 191.

[62] R. M. Balustraitis *et al.* , *Phys. Rev.* **D33** (1986) 629.

[63] J. E. Gaiser *et al.* , *Phys. Rev.* **D34** (1986) 711.

[64] T. M. Himel *et al.* , *Phys. Rev. Lett.* **45** (1980) 1146.

[65] L3 Collaboration, *submission to XXIX Int. Conf. on High Energy Physics,* Vancouver, 1998.

[66] V. Savinov and R. Fulton, (CLEO Collaboration) *Proc. 10th Int. Workshop on Photon-Photon Collisions*, Sheffield, England, 1995, ed. by D. J. Miller *et al.* , (World Scientific, 1995) p. 203.

[67] H. Albrecht *et al.* , *Phys. Lett.* **B338** (1994) 390.

[68] O. Adriani *et al.* , *Phys. Lett.* **B318** (1993) 575.

[69] W-Y. Chen *et al.* , *Phys. Lett.* **B243** (1990) 169.

[70] H. Aihara *et al.* , *Phys. Rev. Lett.* **60** (1988) 2355.

[71] T. A. Armstrong *et al.* , *Phys. Rev. Lett.* **70** (1993) 2988.

[72] Particle Data Group, *Phys. Rev.* **D45** (1992) 1.

[73] J. Dominick *et al.* , (CLEO Collaboration), *Phys. Rev.* **D50** (1994) 4265.

[74] L3 Collaboration, L3 Preprint #165

[75] K. Ackerstaff *et al.* , *Phys. Lett.* **B439** (1998) 197.

[76] D. A. Bauer *et al.* , *Phys. Lett.* **B302** (1995) 345.

[77] M. Ambrogiani *et al.* , submitted to *Phys. Rev. Lett.*

[78] T. K. Pedlar, in *Proc. Workshop on Heavy Quarks at Fixed Target*, Batavia, IL 1998, ed. by J. Butler and H. Cheung, (AIP: New York, 1999), p 369.

[79] R. A. Lee *et al.* , Stanford University Report SLAC-282, (unpublished) 1985.

[80] R. Fulton, Ph.D. dissertation, The Ohio State University (unpublished), 1996.

[81] C. Edwards *et al.* , *Phys. Rev. Lett.* **48** (1982) 70.

[82] A. Martin and J.-M. Richard, *Phys. Lett.* **115B** (1982) 323.

[83] W. Buchmüller, Y. J. Ng and S.-H. H. Tye, *Phys. Rev.* **D24** (1981) 3003.

[84] S. N. Gupta *et al.* , *Phys. Rev.* **D49** (1994) 1551.

[85] X. Q. Zhu *et al.* , *Phys. Rev.* **D47** (1993) 1155.

[86] E. Eichten and C. Quigg, *Phys. Rev.* **D52** (1995) 1726.

[87] Y.-Q. Chen and R. J. Oakes, *Phys. Rev.* **D53** (1996) 5051.

[88] C. Quigg and J. L. Rosner, *Phys. Lett.* **B71** (1977) 153.

[89] Y.-Q. Chen and Y.-P. Kuang, *Phys. Rev.* **D46** (1992) 1165.

[90] K. K. Seth, *priv. comm.*

[91] S. Godfrey and N. Isgur, *Phys. Rev.* **D32** (1985) 189.

[92] E. S. Ackleh and T. Barnes, *Phys. Rev.* **D45** (1992) 232.

[93] J. Linde and H. Snellmann, hep-ph/9703383.

[94] S. N. Gupta, J. M. Johnson and W. W. Repko, *Phys. Rev.* **D54** (1996) 2075.

[95] H-W. Huang, C-F. Qiao and K-T. Chao, *Phys. Rev.* **D54** (1996) 2123.

[96] G. T. Bodwin, E. Braaten and G. P. LePage, *Phys. Rev.* **D46** (1992) R1914, *Phys. Rev.* **D51** (1995) 1125, *Erratum: Phys. Rev.* **D55** (1997) 5853.

[97] H-W. Huang and K-T. Chao, *Phys. Rev.* **D54** (1996) 6850, *Erratum: Phys. Rev.* **D56** (1997) 1821

[98] P. Abreu *et al.* , *Phys. Lett.* **B441** (1998) 479.

[99] T. Barnes, T. E. Browder and S. F. Tuan, *Phys. Lett.* **B385** (1996) 391.

[100] F. Wilczek, in *Proc. XVI International Symposium on Lepton and Photon Interactions,*, Ithaca, NY, 1993, (AIP: New York, 1994), p. 593.

[101] T. A. Armstrong *et al.* , *Nucl. Phys.* **B373** (1992) 35.

[102] S. Bethke, paper presented to the IVth Int. Symp. on Radiative Corrections, Barcelona, 1998, hep-ex/9812026.

[103] M. Jacob and G. C. Wick, *Ann. Phys.* **7** (1959) 404.

[104] A. D. Martin and T. D. Spearman, *Elementary Particle Theory,* North-Holland Publishing Company, Amsterdam, 1970.

[105] W. Baldini, Ph.D. dissertation, University of Ferrara (unpublished), 1998.

[106] J. J. Zhao, Ph.D. dissertation, Northwestern University (unpublished), 1993.

[107] Sheng Jin, E835 memo (unpublished), Feb. 1999.

[108] G. J. Feldman and R. D. Cousins, *Phys. Rev.* **D57** (.) 3873

Appendix A

The CCAL Splitter-Shaper-Discriminator Circuit

A.1 Introduction

With the increased instantaneous luminosity which was expected in E835, event rates in all detectors were expected to increase by up to a factor five over typical rates in E760. These event rates would have caused a large increase in the incidence of pileup, that is, the existence of extra clusters in the CCAL due to multiple interactions occurring within the time defined by a single FERA gate. Pileup clusters, if not identified as such, could cause a good event to be discarded.

There are two solutions which we have employed in E835 to reduce the effect of pileup clusters. First, we use shorter FERA ADC gates. In E760, a 150 ns wide FERA gate was used. It would be impossible to reduce the gate width in E835 unless the $\sim$ 150 ns wide CCAL pulses could be reduced considerably. This was done. Second, in order to identify pileup clusters by timing, TDC's were installed for all 1280 CCAL channels.

Both of these solutions were implemented in E835 by a passive pulse shaping circuit called the Splitter-Shaper-Discriminator Circuit (SSD). The SSD was designed by Jose Marques and FNAL Engineer Claudio Rivetta. In this appendix we describe the testing and performance of the SSD, whose schematic is presented in Fig. A.1, and the setting of final component values for the circuit for each of the four types of CCAL photomultiplier tubes. (three types are indicated in the figure - the $3''$ and $2.5''$ CCAL PMTs use the same circuit components)

A.2 Testing of the SSD Prototype

After basic design work for the SSD was completed, we received a prototype board containing 16 of the circuits for testing. We were concerned about two aspects of the SSD operation. First, it was essential that its response to input pulses be linear. That is, we wanted the output signal from the SSD have an area which was a linear function of the input pulse area, for a large range of input pulse sizes. Second, we wanted to make sure that the SSD pulses were narrow enough so that the goals of pileup minimization could be realized.

A.2.1 Linearity of the SSD

We verified the linearity of the SSD prototype for a large range of input pulse sizes, using a setup represented by the block diagram in Fig. A.2. Light from a nitrogen

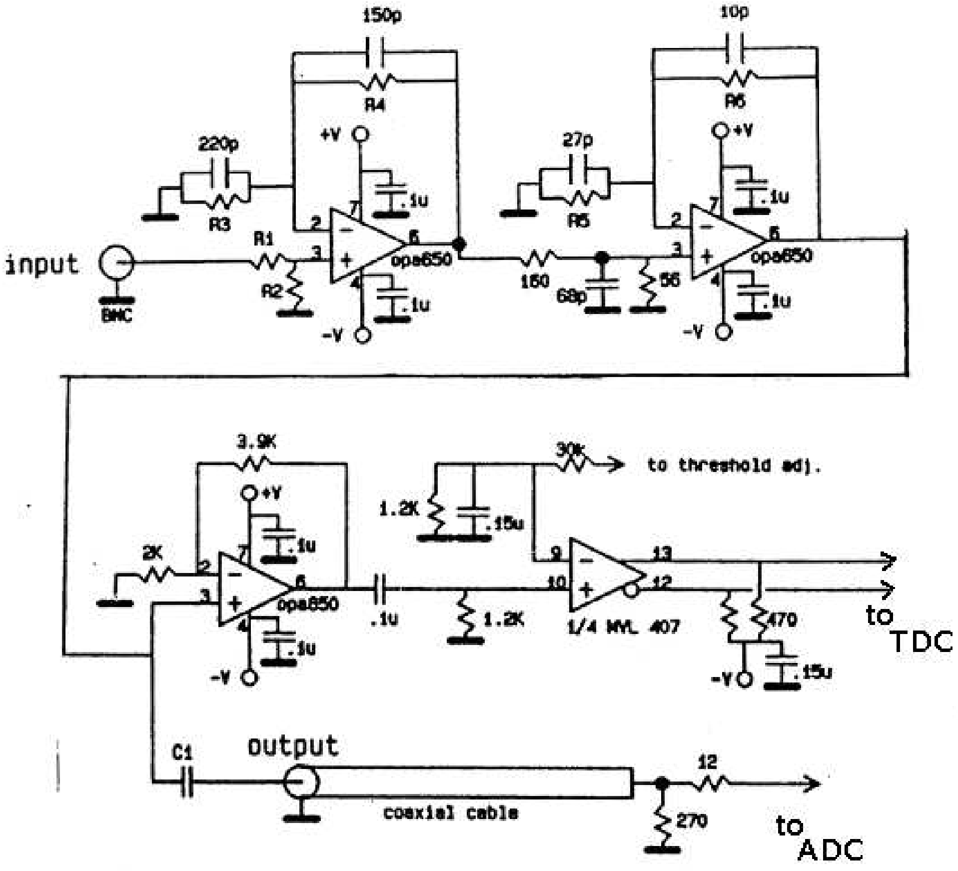

Tube diameter		R1	R2	R3	R4	R5	R6	C1
(3")	1	24	27	1.2K	1.0K	1.3K	1.3K	22nF
(2")	2	30	20	1.2K	680	820	1.5K	22nF
(1.5")	3	30	18	910	680	680	1.5K	18nF

Figure A.1: Schematic diagram of an SSD channel for the shaping of one input signal from a CCAL block.

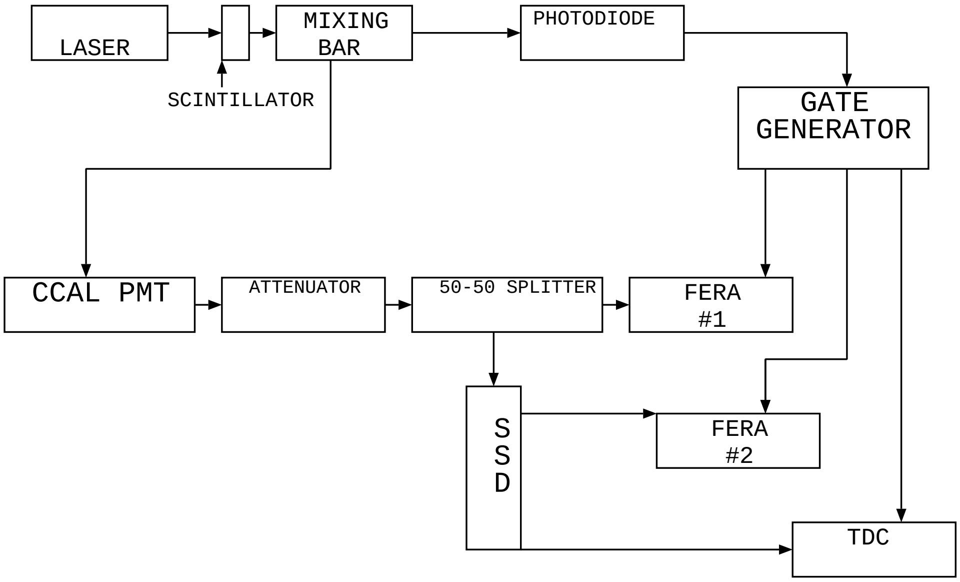

Figure A.2: Test setup for the SSD prototype at FNAL.

laser (Laser Science, Inc. model #VSL-337ND, peak λ = 337 nm) was incident upon a scintillator, which produced blue light. The light pulses were transported via a fiber optic cables to the 1280 CCAL blocks. The output signal from a CCAL PMT was passed through a variable attenuator, and then to a resistor junction, which split the signal into two equal parts. One half of the attenuated signal was then input straight into a FERA, while the other was input into the SSD, and the SSD output was passed into a second FERA.

The linearity of each of the 16 channels of the prototype SSD board was checked by comparing the FERA ADC outputs of the shaped and unshaped signals. This was done for a large range of pulse sizes (approximately 3 to 900 ADC counts). The pulse sizes were changed by changing the attenuator. The ratio of outputs for the shaped to the unshaped pulses for one channel of the prototype SSD is shown in

Fig. A.3. As is apparent from the fit to the data presented in the figure, the circuit is linear to a very good approximation.

A.2.2 Shaped Pulses and Pileup

In E760, the unshaped CCAL pulse at the input of the FERA had a very long tail, or undershoot, caused by distortion of the signal due to its passage through $\sim$ 300 ns of delay cable. With such a pulse shape, an untriggered interaction occurring before a real event trigger resulted in what appeared to be ‘extra’ clusters, which could possibly be confused as due to the triggered event. In the higher rate environment of E835, the background due to these phenomena would have been significantly worse if no improvement to the CCAL signal readout were made. The SSD was used to alleviate this problem in two ways.

First, it shapes pulses such that the tail of the pulse returns to baseline more quickly, and therefore the effect of each untriggered interaction is shorter. We found that the SSD output pulses for even very large ($\sim$ 1000 ADC counts) pulses generally returned to baseline in less than 100 ns. This reflects marked improvement over the unshaped pulses, which remain below baseline for several μsec.

Second, the SSD output pulses have an overshoot rather than an undershoot. The overshoot is not integrated by the FERAs, so ’pileup’ clusters should not occur at all.

Since the input signal shapes for laser pulses are different than those from ’real’ events, the shaped pulses also have different shapes. (See Fig. A.4) In particular, the overshoot for a laser pulse is significantly larger than that for cosmic rays (and

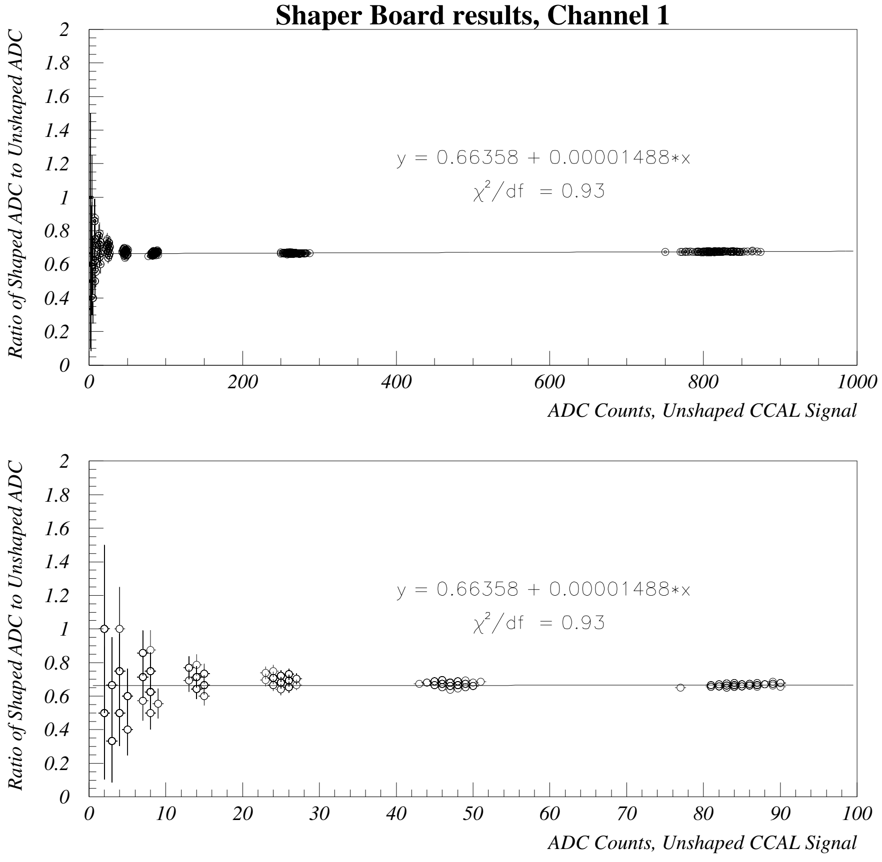

96/05/02 12.20

Figure A.3: Result of linearity test for Channel 1 of the SSD prototype.

for real events, as we found at BNL). As we can see from the figure, the cosmic ray pulse returns substantially to baseline in $\lesssim$ 80 ns.

A.3 Timing of Shaped Pulses

In E760 precise timing information was unavailable for signals from individual CCAL elements. The lack of such information in the higher rate environment of E835 would have been a great problem, so the SSD was designed to provide timing for individual signals as well. This is accomplished in the SSD (see Fig. A.1) by splitting off part of the shaped signal and passing it through a discriminator, whose threshold is adjustable. The discriminated signal from each of the 16 channels on an SSD circuit board is then passed to a corresponding TDC.

A.4 Beam Test at Brookhaven

We took the SSD prototype to the B2 test beam line at the Brookhaven National Laboratory in order to study the SSD prototype performance using ‘real’ events, and to finalize the components on the SSD for production. The beam line delivered an unseparated beam of 3 GeV negatively charged particles; we triggered on electrons by means of the test setup shown in Fig. A.5. Two pairs of crossed scintillator paddles identified the passage of charged particles through a threshold Čerenkov detector, which identified electrons. The coincidence of the five signals (one from each scintillator paddle, and one from the Čerenkov detector) was used to define

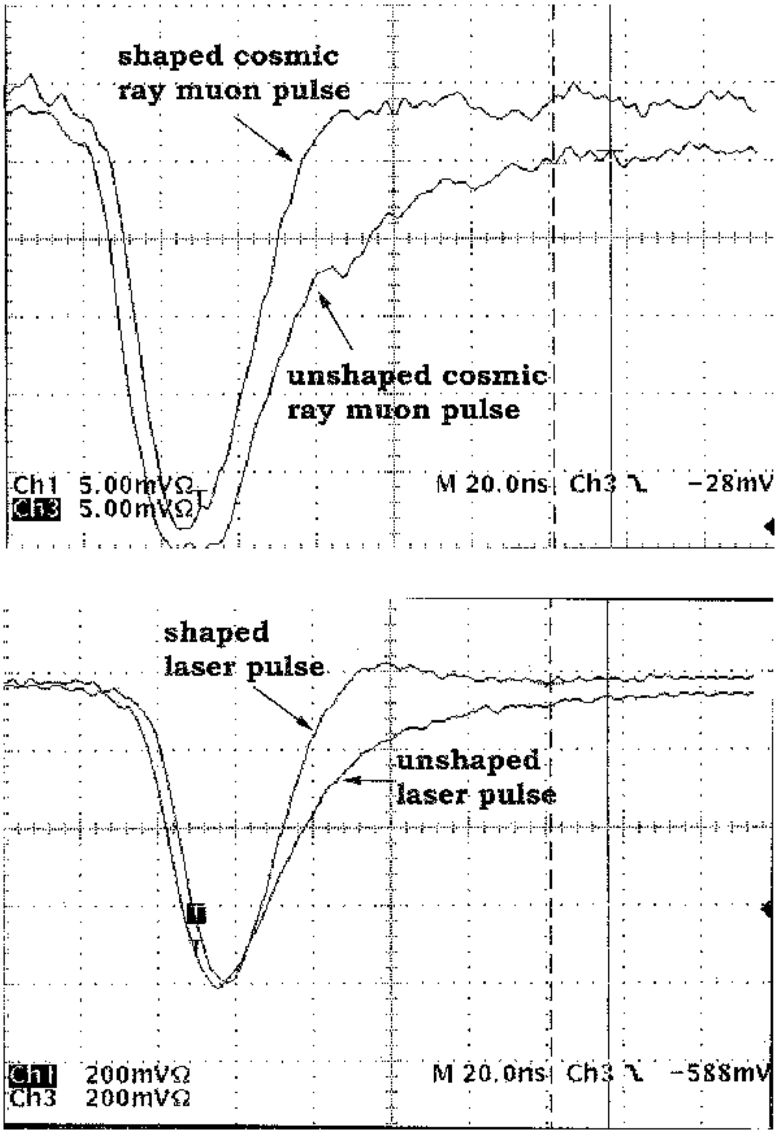

Figure A.4: Comparison of the CCAL signal pulses due to (top) a cosmic ray muon and (bottom) a pulse from the laser system. As noted in Chapter 4, the shape of the two signals is similar enough to enable use of the laser data as a CCAL gain monitor.

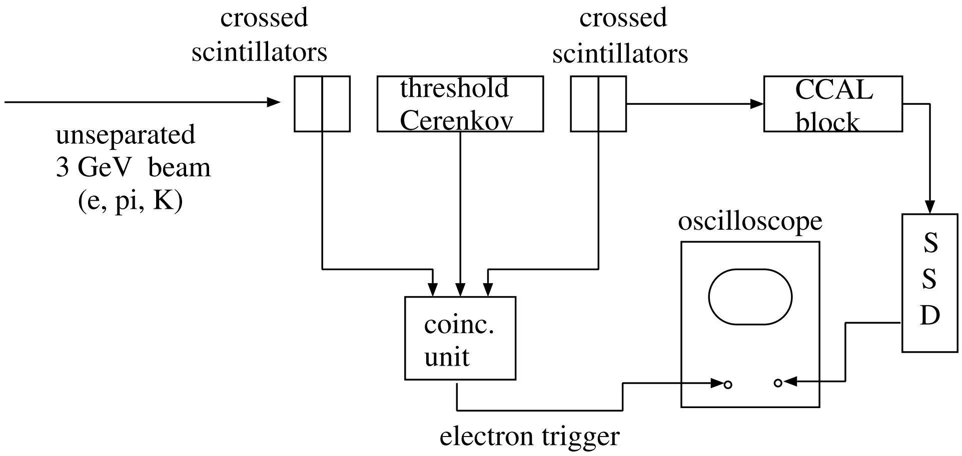

Figure A.5: Setup at Brookhaven for the beam test of the SSD prototype.

the trigger for a digital oscilloscope, to which the CCAL PMT signal was passed. During the test, we optimized the SSD circuit components for each of the PMT sizes ($3'', 2.5'', 2''$ and $1.5''$) which we use in the CCAL. By optimized, we mean the following:

1. The output pulse should be as narrow as practical, i.e. the pulse should cross the baseline as quickly as possible. Narrower pulses allow the use of narrower FERA gates, which is to be preferred.

2. The pulse should have a small overshoot, rather than an undershoot, as was the case in E760. Undershoots can give rise to extra clusters which must be removed by offline analysis, as was mentioned above.

3. The pulse should cross the baseline (and more specifically, the TDC threshold) smoothly; otherwise, the discriminator on the SSD may be tripped falsely, giving rise to false TDC hits.

Table A.1: Results for BNL test of the SSD

Ring (PMT size)	Typical Full Pulse Width	Overshoot %
1-16 (3" & 2.5")	$\sim 70\ ns$	2.1%
17-18 (2")	$\sim 50\ ns$	1.4%
19-20(1.5")	$\sim 45\ ns$	1.5%

4. The overshoot should return to baseline as soon as possible.

We set the final component values for three different SSD circuits; the shape of signals from the $3''$ and $2.5''$ tubes are similar enough that we required only three different circuits rather than four. The final pulse shape is governed by the RC time constants of the two filters in the circuit (the first two elements after the input - see Fig. A.1) and the circuit's overall time constant, which may be varied by changing the output capacitor. During the test, we adjusted these component values "on the fly", as we took data. The original component values had been suggested by using Spice (an electronics simulation package for the PC), and we made adjustments to these values in order to achieve the best pulse shapes for each PMT using the 3 GeV electron pulses. Final component values are shown in the table at the bottom of Fig. A.1.

Appendix B

Performance of the Central Calorimeter (CCAL)

There are several criteria by which the performance of the CCAL may be evaluated. These include energy resolution for individual clusters, angular resolutions in both θ and ϕ, and the variation of CCAL gain (or calibration) constants, which relate the amount of charge collected by the CCAL PMTs to the energy deposited in the attached CCAL blocks.

The energy and angular resolutions are in fact as much measures of the performance of the clusterizing algorithms discussed in Sec. 6.1 as of the intrinsic character of the detector. These resolutions are best determined by studying the characteristics of two body decays. Since two-photon decays $\bar{p}p \rightarrow \gamma\gamma$ are neither prolific in their yield, nor easy to identify, these resolutions are determined using a clean sample of $J/\psi \rightarrow e^+e^-$ events. As was emphasized in Chapter 3, while these resolutions are important in identifying the decay products, they are not of primary importance in determining the precision of our measurements of charmonium state masses and

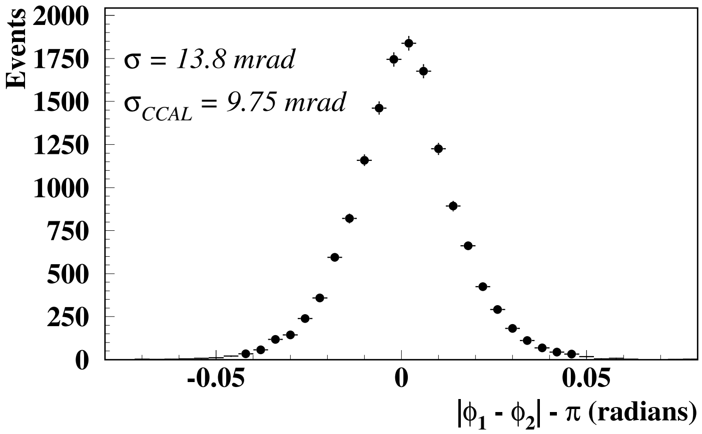

Figure B.1: Azimuthal angle (ϕ) resolution for $J/\psi \rightarrow e^+e^-$ events.

widths precisely.

The gain constant variation is a reflection of the physical changes in the lead glass of the CCAL due to radiation damage or PMT aging. It is monitored by two methods - first, by an iterative procedure with π^0 mass reconstruction, using $\pi^0\pi^0$ events collected at each energy, and second, by means of the data from the laser monitor which was described in Sec. 5.6.

B.1 Angular Resolutions

We are interested in both the azimuthal angle (ϕ) resolution and the polar angle (θ) resolution. The azimuthal angle resolution is rather simple to determine. We discuss it first.

Azimuthal angle (ϕ) Resolution

The resolution for the azimuthal angle ϕ may be determined by examining the deviation from coplanarity of the reconstructed angles ϕ_1 and ϕ_2 of the electrons in the $J/\psi \rightarrow e^+e^-$ event sample. For these events we can construct a plot of the variable $|\phi_1 - \phi_2| - \pi$, which should be a Gaussian function distributed about zero. Fig. B.1 shows the ϕ resolution determined in this manner, and the result of a Gaussian fit to the distribution. The σ_ϕ determined from the fit is simply related to the CCAL resolution for ϕ by $(\sigma(|\phi_1 - \phi_2| - \pi))^2 = (\sigma(\phi_1))^2 + (\sigma(\phi_2))^2 = 2\,(\sigma(\phi))^2$, since the resolution should not depend on ϕ. Thus the fit result of $\sigma_\phi = 13.8$ mrad corresponds to a single cluster resolution of $\sigma_\phi^{CCAL} = 13.8/\sqrt{2} = 9.75$ mrad.

Polar angle (θ) Resolution

In E760 the CCAL polar angle resolution was determined by comparing angles measured by the CCAL to those measured by the charged tracking detectors, whose resolution was significantly better than that of the CCAL. [40] In E835, the scintillating fiber (SF) detector replaces the tracking detectors for θ measurements for the charged particles. For the purposes of this dissertation we are interested in determining the polar angle resolution of the CCAL. This can be done in two ways: measure the overall θ resolution of CCAL by measuring θ of both particles from a two-body decay with the CCAL, or measure θ for one particle in the CCAL and the other in the SF, if that would lead to better results. To make the choice it is necessary to determine the θ resolution of both SF and CCAL. We calculate in this section the resolution for θ of the SF, and compare it to that of the CCAL.

For a two-body process such as $\bar{p}p \rightarrow J/\psi \rightarrow e^+e^-$, there is a simple kinematical relation between the laboratory polar angles θ_1 and θ_2 of the two electrons. We can use the measurement of the angle θ_1 to predict the angle θ_2:

$$\theta_2^{pred} = \sin^{-1}\left(\frac{s \sin\theta_1^{meas}}{E_{TOT}^2 + p_{\bar{p}}^2 - 2E_{TOT}p_{\bar{p}}\cos\theta_1^{meas}}\right). \tag{B.1}$$

The distributions for $f(\theta_1^{meas}, \theta_2^{meas}) \equiv (\theta_2^{meas} - \theta_2^{pred})$ for four different regions of θ_1^{meas} are shown in Fig. B.2, with both electrons detected in either the SF or in the CCAL. It is clear from the figures that the "effective θ resolution" * for the SF is actually poorer than that of the CCAL. This result may appear counter-intuitive, but arises primarily from the finite extension of the interaction region.

The following schematic calculation makes this easy to understand. Figure B.3 illustrates the geometry of particle detection. Let the interaction region be spread uniformly, $\pm a$ about the central point. Let a particle exiting the central target point at an angle θ be detected at a point on the detector. Let the intrinsic uncertainty in this point be $\pm b$ on the detector (SF or CCAL). It can be shown that the extreme angles θ_1 and θ_2 are:

$$\begin{aligned}\theta_1 &= tan^{-1}\left(\frac{r\sin\theta - b\cos\theta}{r\cos\theta + a + b\sin\theta}\right)\\ \theta_2 &= tan^{-1}\left(\frac{r\sin\theta + b\cos\theta}{r\cos\theta - a - b\sin\theta}\right).\end{aligned} \tag{B.2}$$

Let us consider a mid-range polar angle, $\theta = 37.2°$. In this case, for SF, $r \simeq 24.3$ cm, and for CCAL, $r = 131.54$ cm. Let us assume reasonable estimates for b. For

---

[*] as distinguished from the nominal resolution, which depends only on the z position of the detected particle in the SF or CCAL detector

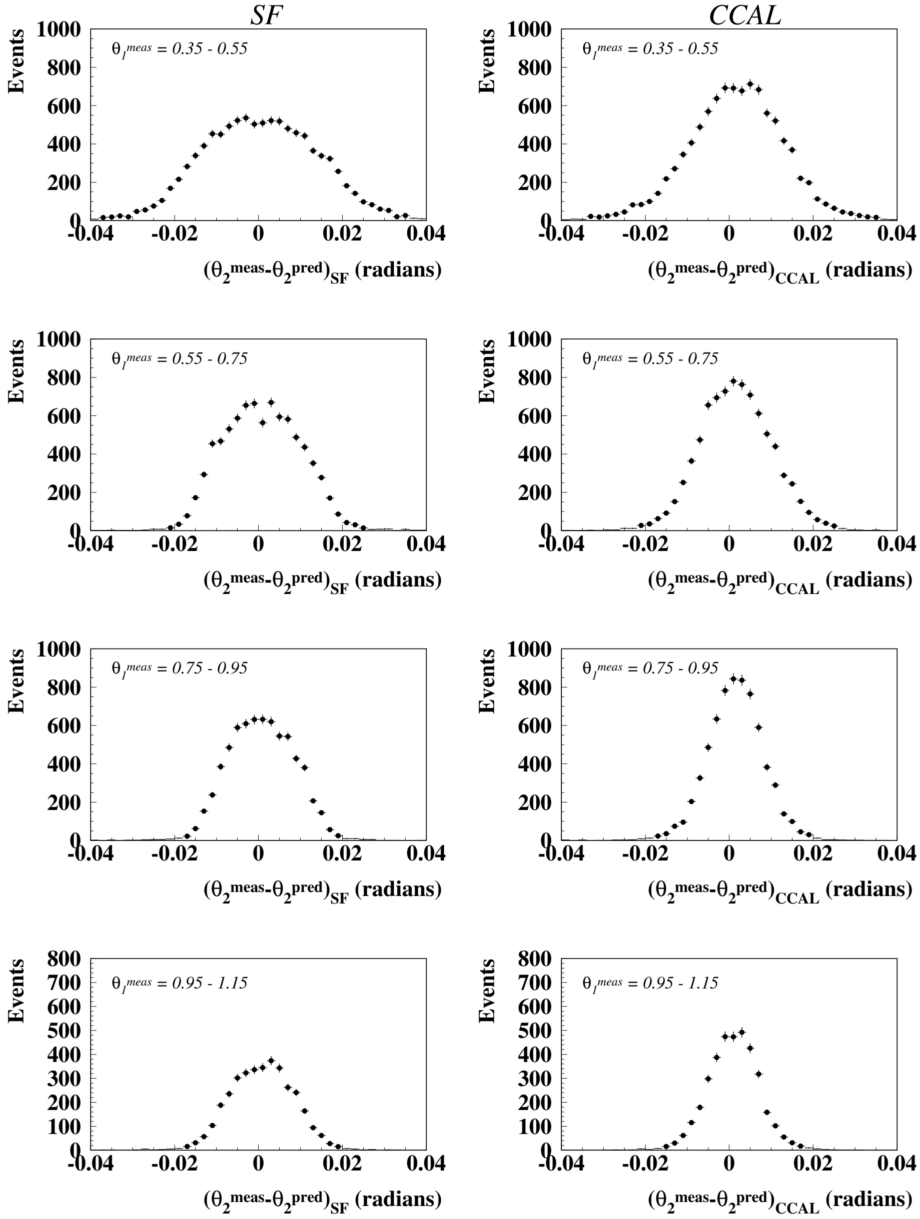

Figure B.2: Distributions of $\theta_2^{meas} - \theta_2^{pred}$ for intervals of θ_1 as measured by the SF (left) and by the CCAL (right).

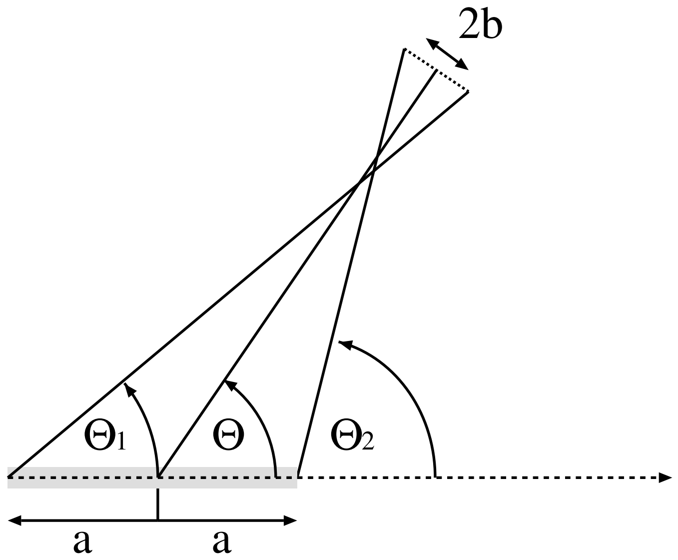

Figure B.3: Schematic showing the geometry of particle detection. The interaction region, of full length $2a$ is indicated by the dots. The uncertainty in the position detection, at the detector, is $\pm b$.

CCAL, $b = 5$mm, and for SF, $b = 0.17$mm. With these values, we find the results shown in Table. B.1.

Table B.1 shows that despite the SF's superior position resolution, when the finite target extension is taken into account, the SF's "effective angular resolution" becomes a factor 2 worse than that of CCAL. This is because the SF is nearer to the

Table B.1: Results of schematic calculation of the effect of finite target region and intrinsic position resolution on the "effective" CCAL and SF resolution for θ.

	with $2a = 0$mm	with $2a = 10$mm
θ(CCAL)	$37.2^\circ \pm 0.22^\circ$	$37.2^\circ \pm 0.35^\circ$
θ(SF)	$37.2^\circ \pm 0.04^\circ$	$37.2^\circ \pm 0.74^\circ$

interaction region by more than a factor five. This conclusion is borne out by a more realistic Monte Carlo calculation considering a more realistic Gaussian distribution for the uncertainty in position resolution for both SF and CCAL.

In view of the above, we have decided to use the measurements of both θ_1 and θ_2 in CCAL in order to estimate the θ resolution of CCAL.

The resolution σ_θ^{CCAL} is not given simply by the standard deviation of the distributions shown in Fig. B.2. The error on $f = \theta_2^{meas} - \theta_2^{pred}$ is given by:

$$\sigma_f^2 = \sigma^2(\theta_2^{meas}) + \sigma^2(\theta_2^{pred}), \tag{B.3}$$

We obtain $\sigma(\theta_2^{pred})$ by differentiating Eq. B.1:

$$\sigma(\theta_2^{pred}) = \sigma(\theta_1^{meas}) \times \left[\frac{\left(\frac{A\cos\theta_1^{meas} - B}{A - B\cos\theta_1^{meas}}\right)}{\sqrt{(A^2-1) + (B^2+1)\cos^2\theta_1^{meas} - 2AB\cos\theta_1^{meas}}} \right], \tag{B.4}$$

where $A = (E_{TOT}^2 + p_{\bar{p}}^2)/s$ and $B = 2E_{TOT}p_{\bar{p}}/s$.

We can write Eq. B.4 as $\sigma(\theta_2^{pred}) = g(\theta_1^{meas})\sigma(\theta_1^{meas})$, where $g(\theta_1^{meas})$ is the expression in the square brackets. Thus,

$$\sigma_f^2 = \sigma^2(\theta_2^{meas}) + g(\theta_1^{meas})^2\sigma^2(\theta_1^{meas}). \tag{B.5}$$

In Fig. B.4 we have plotted σ_f as a function of θ_2. The σ_f were obtained by fitting the individual distributions of $f = \theta_2^{meas} - \theta_2^{pred}$ for small intervals of θ_1^{meas}. (as illustrated in Fig. B.2 for larger intervals of θ_1^{meas}) Then, we fitted the σ_f as a function of θ_1^{meas}, and found that the observed shape could be accomodated by errors $\sigma(\theta_{1,2}^{meas})$ which were linear functions of $\theta_{1,2}^{meas}$: $\sigma(\theta_{1,2}^{meas}) = \alpha + \beta \times \theta_{1,2}^{meas}$. The result of this fit to the σ_f is shown in Fig. B.4.

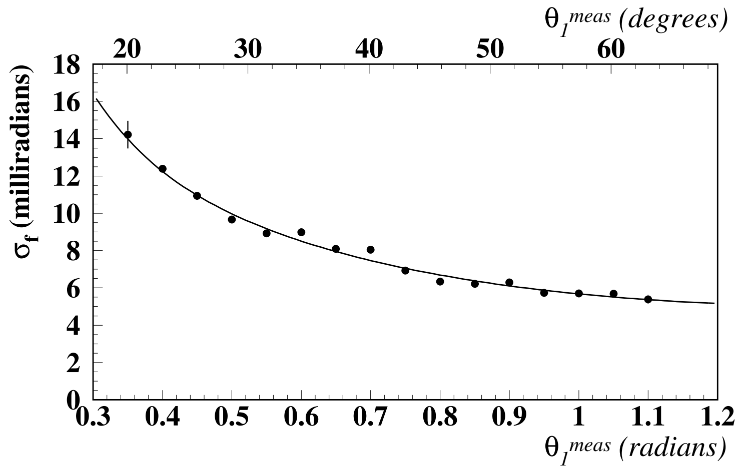

Figure B.4: The distribution of the standard deviation σ_f of $f = \theta_2^{meas} - \theta_2^{pred}$ as a function of θ for electrons from $\bar{p}p{\rightarrow}J/\psi{\rightarrow}e^+e^-$ events. The curve is the result of a fit to the σ_f assuming that $\sigma(\theta_{1,2}^{meas}) = \alpha + \beta\theta_{1,2}^{meas}$.

We may also wish to estimate the $\sigma(\theta_{1,2}^{meas})$ by the schematic calculation method we used previously. In Table B.2 we show the results, assuming reasonable position errors $b = 2mm$ at $\theta = 20°$ and $b = 7mm$ at $\theta = 65°$.

Finally, in Fig. B.5 we have plotted the results for $\sigma(\theta_{1,2}^{meas})$ obtained by the fit to σ_f and by the schematic method. The real errors $\sigma(\theta_{1,2}^{meas})$ probably lie somewhere between the two lines.

Table B.2: Results of the schematic calculation of “effective” CCAL resolutions for θ at 20° and 65°, using $a = 5$mm. Here we have assumed a varying CCAL position error b.

$\theta_{nominal}$	b	r	θ
20°	2 mm	196.3 cm	$20° \pm 0.11°$
65°	7 mm	89.44 cm	$65° \pm 0.74°$

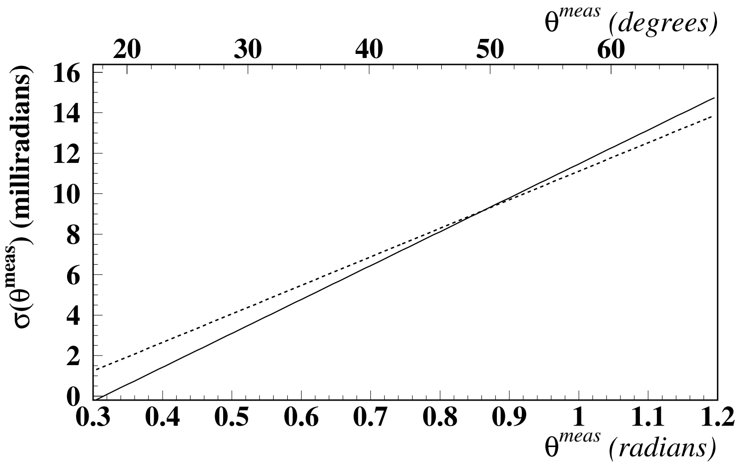

Figure B.5: The results of two estimates of the dependence of the errors $\sigma(\theta^{meas})$ on θ^{meas}. The solid line is the result of a fit to the measured σ_f assuming that $\sigma(\theta_{1,2}^{meas}) = \alpha + \beta\theta_{1,2}^{meas}$. The dashed line is a result of using the schematic method, assuming a position error $b = 2mm$ at $\theta = 20°$ and $b = 7mm$ at $\theta = 65°$.

B.2 Energy Resolution

The average energy resolution of the CCAL for large energy clusters can similarly be examined using $J/\psi \to e^+e^-$ events. The predicted energy of an electron in a $J/\psi \to e^+e^-$ decay is given by

$$E_{e^-}^{pred} = \frac{s}{2(E_{TOT} - p_{\bar{p}} \cos\theta_{e^-}^{meas})}. \tag{B.6}$$

Differentiating this with respect to θ_{e^-}, we obtain

$$\sigma(E_{e^-}^{pred}) = \frac{(s \times p_{\bar{p}}/2E_{TOT}^2)\sin\theta_{e^-}^{meas}}{(1 - (p_{\bar{p}}/E_{TOT})\cos\theta_{e^-}^{meas})^2}\sigma(\theta_{e^-}^{meas}) \equiv \mathcal{F}(\theta_{e^-})\sigma(\theta_{e^-}^{meas}) \tag{B.7}$$

and therefore, the error on the quantity $\Delta E = E_{e^-}^{meas} - E_{e^-}^{pred}$ is given by

$$\sigma^2(\Delta E) = \sigma_{E^{meas}}^2 + \sigma_{E^{pred}}^2 = \sigma_{E^{meas}}^2 + \mathcal{F}^2(\theta_{e^-}^{meas})\sigma^2(\theta_{e^-}^{meas}) \tag{B.8}$$

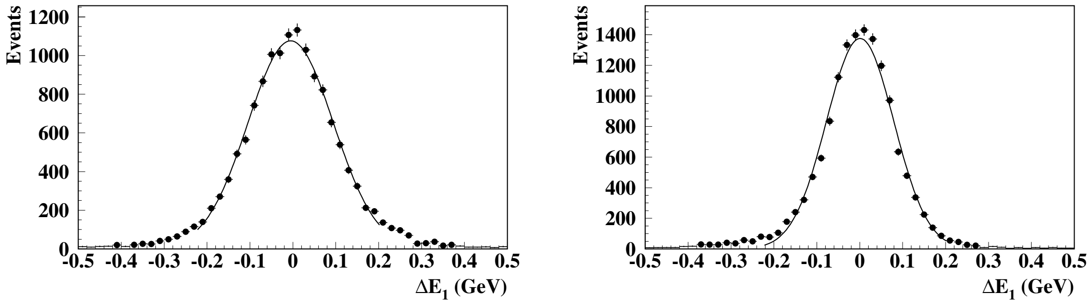

Figure B.6: Average energy resolution for electrons from $J/\psi \rightarrow e^+e^-$ events with average energy (left) $E \simeq 2$ GeV and (right) $E \simeq 3.1$ GeV. The curves are the result of fits to the data. For each, $\sigma_E \approx 5.6\% \times \sqrt{E}$.

Over the range of angles covered by the CCAL, $\sim 20°$ to $\sim 65°$, the expected energies are 4.2 GeV to 1.3 GeV. Given the resolution for θ^{meas} in Table B.2, and the result of Eq. B.7, the error $\sigma(E^{pred})$ ranges from $\sim$ 8 to $\sim$ 22 MeV. This error can be neglected in comparison to $\sigma(E^{meas})$, which was found in E760 to be $\sim 6\% \times \sqrt{E^{meas}} \simeq 70 - 110$ MeV. (see, *e.g.,* Ref. [101]) Roughly, the error $\sigma(\Delta E)$ can be expected to be equal to $\sigma(E^{meas})$ for these large energy clusters. The distributions of Δ_E for $J/\psi \rightarrow e^+e^-$ events for average electron energies $\langle E \rangle = 2$ GeV and $\langle E \rangle = 3.1$ GeV is shown in Fig. B.6. We have fit each to a Gaussian function, and each fit results in a standard deviation $\sigma_{E^{meas}}$ of $\sim 5.6\% \times \sqrt{E}$. This is consistent with the average energy resolution found in E760.

More important for our studies is the energy resolution for low energy photons. Our greatest concern is that low energy photons from asymmetric $\pi^0 \rightarrow \gamma\gamma$ decays are detected with sufficient energy resolution so that the two photons may be reconstructed as a π^0. We can check that this is the case by examining the distribution

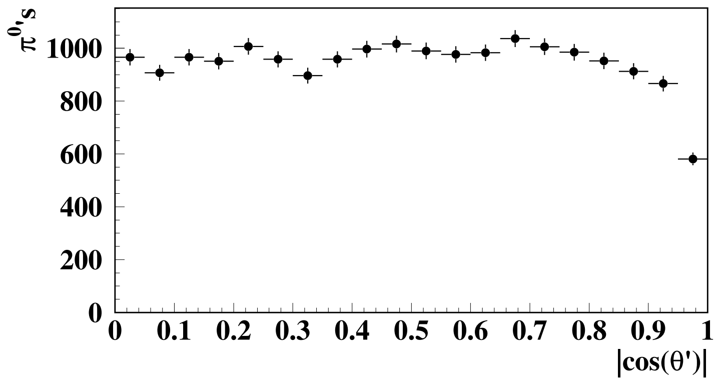

Figure B.7: Number of reconstructed π^0's as a function of $|\cos\theta'|$, where θ' is the angle of one of the photons in the π^0 reference frame. The dip at $|\cos\theta'| \simeq 1$ indicates that asymmetric decays are being lost.

of reconstructed π^0 events as a function of the angle θ' of one of the photons in the π^0 reference frame, measured relative to the π^0 direction. This angle is expressed simply as $(\cos\theta') = (E_1 - E_2)/(\beta_{\pi^0}(E_1 + E_2))$, where β_{π^0} is the speed of the π^0 in the center of mass frame. Since π^0's decay isotropically, we expect that this distribution is flat in $\cos\theta'$. If the measured distribution shows a deviation from isotropy near $|\cos\theta'| = 1$, it indicates a problem of reconstructing asymmetric π^0 decays. If a deviation from isotropy is seen near $|\cos\theta'| = 0$, then a problem of reconstructing symmetric decays is indicated.

The $\cos\theta'$ distribution for $\pi^0\pi^0$ events collected at $\sqrt{s} = 2990$ MeV is shown in Fig. B.7. There is no noticeable drop-off in the distribution near $|\cos\theta'| = 0$, and we can therefore conclude that the symmetric decays are being reconstructed correctly. There is a drop, however, in the distribution near $|\cos\theta'| = 1$. We believe that this drop-off is due to the asymmetric π^0 decays in which a photon is lost. It therefore provides an indication of the level of feed-down background to expect from $\pi^0\pi^0$ and $\pi^0\gamma$ mimicking $\gamma\gamma$.

B.3 CCAL Gain Variation

The gain constant (or calibration constant) for a CCAL block is the coefficient G in the relation $E_i = G_i \times A_i$, where E_i is the energy deposited in the block by an incident electron or photon, and A_i is the charge collected by the PMT, measured in ADC counts by the FERA. *Constant,* perhaps, is not the proper term, since as time passes, this *constant* changes, either due to PMT aging or radiation damage of the lead glass.

Gross monitoring of the CCAL gains was provided in E835 by a laser system which pulsed each block at a constant rate throughout the run. Fine monitoring and calibration was performed by examination of $\pi^0\pi^0$ events on a stack-by-stack basis, as was done in E760. We describe each of these techniques briefly here.

B.3.1 Laser Monitoring

Gross variations of the CCAL gains were monitored by use of data from the laser monitor trigger (See Sec. 5.6). For each data run, there were $\sim$ 1000 laser triggers recorded, by which the average response of each CCAL channel could be determined. This system provided a relative run-by-run diagnostic on each CCAL channel, though it was good only for large variations ($\gtrsim$ 5%), limited primarily by statistics. Unfortunately, while the laser was capable of pulse rates up to 200 times faster than we used (0.1 Hz) the scintillator which produced visible blue light from the laser's incident UV pulses suffered degradation of light output at rates higher than about 1 Hz. Variation of light output from the laser/scintillator system was not a concern in and of itself, since the pulses were also observed by a pair of photodiodes for normalization purposes. However, the loss in absolute intensity at high pulse rates was too rapid and too large for a higher-statistics sample to be obtained for each run. The intent behind the laser system, though, was only to provide a monitor for gross-scale variations in the CCAL gain constants, which it did satisfactorily.

B.3.2 Gain Constant Calculation

The prolific $\bar{p}p \rightarrow \pi^0\pi^0$ reaction offers us a nice means of calibrating the CCAL, though it requires a somewhat tedious iterative procedure. Most of this work, described in an E835 collaboration memo, [107], was done by our colleague Sheng Jin, using the procedure described in Ref. [106].

The method begins by selecting a clean sample of $\pi^0\pi^0$ events from the stack for which gain constants are required. The measurement of the angles θ and ϕ of one π^0 in the event are taken as a given, and then using two-body kinematics, the other π^0's energy and angles are predicted. A χ^2 function is calculated,

$$\chi^2 = \sum_{i=1} n \frac{\sum_{j=1} m (g_j A_{ij} - E_i)^2}{\sigma_i}, \tag{B.9}$$

where the sum with index j is performed over the number of blocks in the two γ

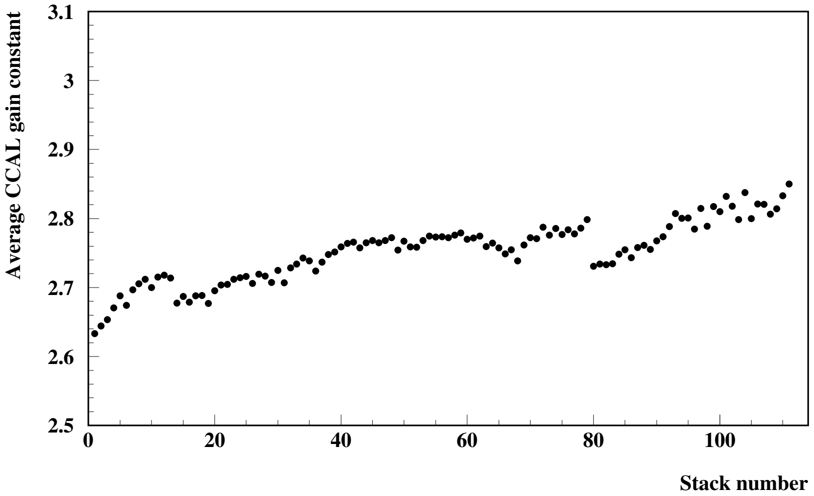

Figure B.8: Variation of the average CCAL channel gain constant, from the beginning of the E835 run (Stack 1) to the end (Stack 110). The general upward trend of the gain constants indicates the darkening the CCAL lead glass blocks due to accumulated radiation dosage during the run.

clusters for a given π^0, and the sum with index i is over all π^0 in the $\pi^0\pi^0$ events. g_j is the gain constant for the jth block, A_{ij} is the number of ADC counts for the jth block of the ith π^0, and σ_i is the energy error estimated from the formula $\sigma_i = 6\%/\sqrt{E(GeV)} + 1.4\%$. This χ^2 function is then minimized with respect to the g_j, and then the newly-calculated gain constants are used to recalculate energies E_i, and the procedure iterated until the g_j converge. Throughout, the masses of the π^0 are constrained to $M(\pi^0) = 139.57$ MeV.

Over the course of the E835 run, 110 stacks were used to calculate gain constants. The variation of the average CCAL channel gain constant is plotted in Fig. B.8 in order to show the change due to radiation damage and/or PMT aging. The general trend of the constants is upward, consistent with the hypothesis that accumulated radiation dosage darkens the lead glass (i.e. decreases the light collected by the CCAL PMTs per unit energy deposited in a block). The discrete drop of $\sim 1\%$ at stack 13 corresponds to a long shutdown in December 1996, during which it is possible that the lead glass cured slightly. The larger drop ($\sim 2\%$) at stack 80 is not understood.

Appendix C

Angular Distribution of the Reactions $\bar{p}p \to \eta_c \to \gamma\gamma$ and $\bar{p}p \to \chi_2 \to \gamma\gamma$

In order to evaluate the efficiency of a cut on the variable $\cos(\theta^*)$ for the processes $\bar{p}p \to \eta_c \to \gamma\gamma$ and $\bar{p}p \to \chi_2 \to \gamma\gamma$, we need to know the angular distribution for the reactions.

The angular distribution for η_c, since it is a pseudoscalar state, is necessarily isotropic. The efficiency of the cut $|\cos(\theta^*)| \leq 0.2$ for $\eta_c \to \gamma\gamma$ region is therefore 0.2.

The $\bar{p}p \to \chi_2 \to \gamma\gamma$ process does not have an isotropic angular distribution, however, but it can be calculated following the formalism of Jacob and Wick. [103]. The organization of this section follows a similar discussion in Ref. [48]

$\underline{\bar{p}p \to \chi_2}$

The two-particle helicity state describing the initial $\bar{p}$ and p can be written as a single ket, $|\theta, \phi; \lambda_1, \lambda_2\rangle$, where θ and ϕ are the angles defining the direction of the $\bar{p}$

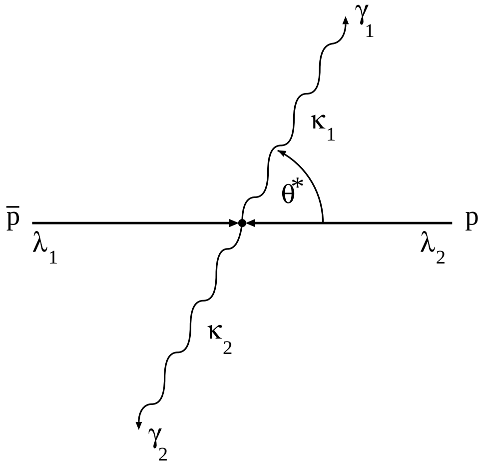

Figure C.1: Schematic of the reaction $\bar{p}p \rightarrow \chi_2 \rightarrow \gamma\gamma$. λ_1 and λ_2 are the helicities of the $\bar{p}$ and p, respectively, while κ_1 and κ_2 are the helicities of the outgoing photons. θ^* is the angle in the CM frame between the incoming $\bar{p}$ momentum and one of the photons.

in the CM frame, and λ_1 and λ_2 are the helicities of the $\bar{p}$ and p, respectively. We can write this state more conveniently by expanding over a complete set of angular momentum states, a là Jacob and Wick, [103]:

$$|\theta, \phi; \lambda_1, \lambda_2\rangle = \sum_{J,M,\lambda_1',\lambda_2'} |J', M'; \lambda_1', \lambda_2'\rangle\langle J', M'; \lambda_1', \lambda_2'|\theta, \phi; \lambda_1, \lambda_2\rangle. \tag{C.1}$$

We note that the second term is given by

$$\langle J', M'; \lambda_1', \lambda_2'|\theta, \phi; \lambda_1, \lambda_2\rangle = \left(\frac{2J'+1}{4\pi}\right)^{1/2} \delta_{\lambda_1\lambda_1'}\delta_{\lambda_2\lambda_2'}\mathcal{D}^{J'}_{M',\lambda}(\phi, \theta, -\phi), \tag{C.2}$$

where $\lambda = \lambda_1 - \lambda_2$. Then, inserting this into Eq. C.1, we have

$$|\theta, \phi; \lambda_1, \lambda_2\rangle = \sum_{J',M'} \left(\frac{2J'+1}{4\pi}\right)^{1/2} \mathcal{D}^{J'}_{M',\lambda}(\phi, \theta, -\phi), |J', M'; \lambda_1, \lambda_2\rangle \tag{C.3}$$

Similarly, we can write the angular momentum state of the χ_2 as $|J, M\rangle$. We note at this point that when calculating the amplitude for $\bar{p}p \rightarrow \chi_2$, the sum over J' and

M' becomes equal to the single term with $J' = J = 2$ and $M' = M$, by angular momentum conservation. Then the amplitude for the formation reaction $\bar{p}p \to \chi_2$ is given by:

$$A(\bar{p}p \to \chi_2) = \langle 2, M|A|\theta, \phi; \lambda_1, \lambda_2\rangle = \left(\frac{5}{4\pi}\right)^{1/2} A_{\lambda_1,\lambda_2} \mathcal{D}^2_{M,\lambda}(\phi, \theta, -\phi), \tag{C.4}$$

where $A_{\lambda_1,\lambda_2} = \langle 2, M|A|2, M; \lambda_1, \lambda_2\rangle$. Here, the definition of D is useful to recall. It is

$$\mathcal{D}^J_{m_1,m_2}(\alpha, \beta, \gamma) = e^{-im_1\alpha} d^J_{m_1,m_2}(\beta) e^{-im_2\gamma}. \tag{C.5}$$

We can choose our axes such that $\phi = 0$, which allowing us to write Eq. C.4 in terms of the d functions alone (which can be found in Ref. [2]):

$$A(\bar{p}p \to \chi_2) = \left(\frac{5}{4\pi}\right)^{1/2} A_{\lambda_1,\lambda_2} d^2_{M,\lambda}(\theta). \tag{C.6}$$

$\underline{\chi_2 \to \gamma\gamma}$

Following reasoning similar to that in the above section, we can write the amplitude for the decay process as (again, refer to Fig. C.1 for definitions):

$$\begin{aligned} A(\chi_2 \to \gamma\gamma) &= \langle \theta^*, \phi^*; \kappa_1, \kappa_2|B|2, M\rangle & \text{(C.7)} \\ &= \left(\frac{5}{4\pi}\right)^{1/2} B^*{}_{\kappa_1,\kappa_2} \mathcal{D}^{*2}_{M,\kappa}(\phi^*, \theta^*, -\phi^*), & \text{(C.8)} \end{aligned}$$

where $\kappa = \kappa_1 - \kappa_2$ and the angles θ^* and ϕ^* are CM angles for one of the two photons.

The evaluation of this amplitude is simpler than the previous one, for the χ_2 quantization axis can be chosen to lie along the line formed by the two photon momenta (thus $\theta^* = 0$). Then, angular momentum conservation requires $\kappa = M$.

and thus

$$\langle \theta^*, \phi^*; \kappa_1, \kappa_2 | B | 2, M \rangle = \left(\frac{5}{4\pi} \right)^{1/2} {B^*}_{\kappa_1,\kappa_2} {\mathcal{D}^*}^2_{M,M}(\phi^*, 0, -\phi^*). \tag{C.9}$$

Again using Eq. C.5, we find that ${\mathcal{D}^*}^2_{M,\kappa}(\phi^*, 0, -\phi^*) = d^2_{M,M}(0) = \delta_{M,M} = 1$. Thus

$$\langle \theta^*, \phi^*; \kappa_1, \kappa_2 | B | 2, M \rangle = \left(\frac{5}{4\pi} \right)^{1/2} {B^*}_{\kappa_1,\kappa_2}. \tag{C.10}$$

$\bar{p}p \rightarrow \chi_2 \rightarrow \gamma\gamma$

The amplitude for the complete reaction $\bar{p}p \rightarrow \chi_2 \rightarrow \gamma\gamma$ is simply given by the product of the partial amplitudes, i.e.

$$A(\bar{p}p \rightarrow \chi_2 \rightarrow \gamma\gamma) = \frac{5}{4\pi} {B^*}_{\kappa_1,\kappa_2} A_{\lambda_1,\lambda_2} d^2_{M,\lambda}. \tag{C.11}$$

Our goal is the calculation of the angular distribution for this process. We can derive it from the differential cross section, which follows in a straightforward manner from the amplitude, averaging over initial spins and summing over the final spins:

$$\frac{d\sigma}{d\Omega}(\bar{p}p \rightarrow \chi_2 \rightarrow \gamma\gamma) \propto \frac{1}{4} \sum_{\kappa_1,\kappa_2} \sum_{\lambda_1,\lambda_2} |A(\bar{p}p \rightarrow \chi_2 \rightarrow \gamma\gamma)|^2. \tag{C.12}$$

Evaluating the amplitudes

In order to determine $d\sigma/d\Omega$, we must evaluate the amplitudes A_{λ_1,λ_2} and B_{κ_1,κ_2}. The number of amplitudes is small (8), and further, the strong and electromagnetic interactions which govern the $\bar{p}p \rightarrow \chi_2 \rightarrow \gamma\gamma$ process respect both time reversal and parity invariance. These lead (see, e.g. Ref. [104]) to a reduction by a factor of two in the number of independent amplitudes:

$$A_{\lambda_1,\lambda_2} = A_{-\lambda_1,-\lambda_2} \text{ and } B_{\kappa_1,\kappa_2} = B_{-\kappa_1,-\kappa_2} \tag{C.13}$$

As a result, we may specify the amplitudes by the value of the initial and final state helicities: the initial state helicity may be 0 or 1 (i.e. λ_1 and λ_2 may take values of $\pm 1/2$), and the final state helicity may be 0 or 2 (since real photons may have only helicities ± 1). Thus, we use the following notation:

$$A_0 = A_{\pm 1/2, \mp 1/2} \qquad A_1 = A_{\pm 1/2, \pm 1/2} \tag{C.14}$$

$$B_0 = B_{\pm 1, \mp 1} \qquad B_2 = B_{\pm 1, \pm 1} \tag{C.15}$$

Now, using the properties of the d function, namely,

$$d^J_{m,n} = (-1)^{n-m} d^J_{n,m} = d^J_{-n,-m}, \tag{C.16}$$

we obtain

$$\begin{aligned} \frac{d\sigma}{d\Omega} &\propto A_0^2 \left[B_0^2 (d^2_{0,0}(\theta))^2 + B_2^2 (d^2_{2,0}(\theta))^2 \right] \\ &+ A_1^2 \left[B_0^2 (d^2_{1,0}(\theta))^2 + B_2^2 \{ \frac{1}{2} (d^2_{2,1}(\theta))^2 + \frac{1}{2} (d^2_{2,-1}(\theta)) \}^2 \right]. \end{aligned} \tag{C.17}$$

The relevant d functions are: [2]

$$\begin{aligned} d^2_{0,0}(\theta) &= \frac{3}{2}\cos^2\theta - \frac{1}{2} \\ d^2_{1,0}(\theta) &= -\sqrt{\frac{3}{2}} \sin\theta\cos\theta \\ d^2_{2,0}(\theta) &= \frac{\sqrt{6}}{4}\sin^2\theta \\ d^2_{2,\pm 1}(\theta) &= -\left(\frac{1 \pm \cos\theta}{2} \right) \sin\theta. \end{aligned} \tag{C.18}$$

Substituting these into Eq. C.17, we find:

$$\begin{aligned} \frac{d\sigma}{d\Omega} &\propto \left(18A_0^2B_0^2 + 3A_0^2B_0^2 - 12A_1^2B_0^2 - 2A_1^2B_2^2 \right) \times \cos^4\theta \\ & \left(12A_1^2B_0^2 - 6A_0^2B_2^2 - 6A_0^2B_0^2 \right) \times \cos^2\theta \\ & \left(2A_0^2B_0^2 + 3A_0^2B_2^2 + 2A_1^2B_2^2 \right) \end{aligned}$$

Helicity states contributing to the process $\bar{p}p \rightarrow \chi_2 \rightarrow \gamma\gamma$

As noted earlier, there are two possible helicities for the initial state (0 or 1) and two for the final state (0 or 2). It has been shown in both E760 and E835, using data for the $\bar{p}p \rightarrow \chi_2 \rightarrow \gamma J/\psi$ reaction, that the initial state of $\bar{p}$ and p predominantly is helicity 1. A 90% CL upper limit of 26% has been placed on the helicity 0 component. [52] The $\chi_2 \rightarrow \gamma\gamma$ decay is predicted to be primarily helicity 2, with at most a 5% contribution from helicity 0. [53]

If we assume purely helicity 1 formation and helicity 2 decay, we have $A_0^2 = B_0^2 = 0$, and the differential cross section becomes:

$$\frac{d\sigma}{d\Omega} = A_1^2 B_2^2 (1 - \cos^4\theta). \tag{C.19}$$

The angular distribution under this assumption, then, is

$$W(\theta) = \mathcal{N}(1 - \cos^4\theta). \tag{C.20}$$

The normalization factor $\mathcal{N}$ is obtained by setting the integral $\int_0^1 W(\theta) d(\cos\theta)$ to 1. This leads to

$$W(\theta) = \frac{5}{4}(1 - \cos^4\theta). \tag{C.21}$$

We assumed this angular distribution in calculating the efficiency of the cut in $\cos\theta^*$ for $\bar{p}p \rightarrow \chi_2 \rightarrow \gamma\gamma$.

Appendix D

Statistical Considerations

1. Statistical Errors

It is standard practice to calculate errors on counts according to Poisson statistics. The confidence limits at various levels: 68.27%, 90%, 95%, 99%, etc., have been recently tabulated by Feldman and Cousins [108] for total number of events observed, $n_{obs} = 0$ to 20, with known mean background levels of 0 to 15. Throughout this dissertation, we use these tables to obtain standard 68.27% statistical errors when the total number of counts in any measurement is less than 20. When the total number of events is greater than 20, the Poisson distribution is well approximated by the Normal distribution, and the statistical error on n_{obs} is taken as $\sqrt{n_{obs}}$.

2. Propagation of Errors

Generally, statistical errors and systematic errors are propagated separately. For the propagation of statistical errors, the usual procedures are followed when the fractional errors are small : $\epsilon(a \pm b) = \sqrt{\epsilon^2(a) + \epsilon^2(b)}$, $f\epsilon(a/b, ab) = \sqrt{f\epsilon^2(a) + f\epsilon^2(b)}$, $f\epsilon(a^n) = n \times f\epsilon(a)$, where ϵ and $f\epsilon$ denote absolute and fractional errors, respectively.

When fractional errors are large, these simple expressions are not correct. The correct procedure often results in asymmetric errors on a function of (a, b) even when the individual errors on a and b are each symmetric. As an example, if a has symmetric errors of $\pm 30\%$, $1/a$ acquires asymmetric errors of ${}^{+42.8\%}_{-23.1\%}$.

The fact that this method is proper may be illustrated as follows. A Gaussian distribution for x is shown in Fig. D.1. 68.3% of the area beneath the curve is found between the mean μ and $\mu \pm \sigma$. This function has a variance σ which is 30% of the mean μ. The distribution for $1/x$, also shown in Fig. D.1, illustrates the problem. While the mean of the distribution is indeed $1/\mu$, the shape of the distribution is highly asymmetric. Upon integrating this curve, we find that 68.3% of the area lies between $1/(\mu+\sigma)$ and $1/(\mu-\sigma)$. Thus we would properly quote the 68.3% confidence interval for $1/x$ as $[1/(\mu+\sigma), 1/(\mu-\sigma)]$. As mentioned above, if $\sigma = 0.3 \times \mu$, the errors on $1/x$ are $+42.8\%$ and -23.1%.

Therefore, when we calculate the branching ratio $B(c\bar{c}\to\gamma\gamma)$ from our determination of the branching ratio product $B(c\bar{c}\to p\bar{p}) \times B(c\bar{c}\to\gamma\gamma)$ by dividing by $B(c\bar{c}\to\bar{p}p)$ with large fractional error, we quote errors on $B(c\bar{c}\to\gamma\gamma)$ with these considerations in mind.

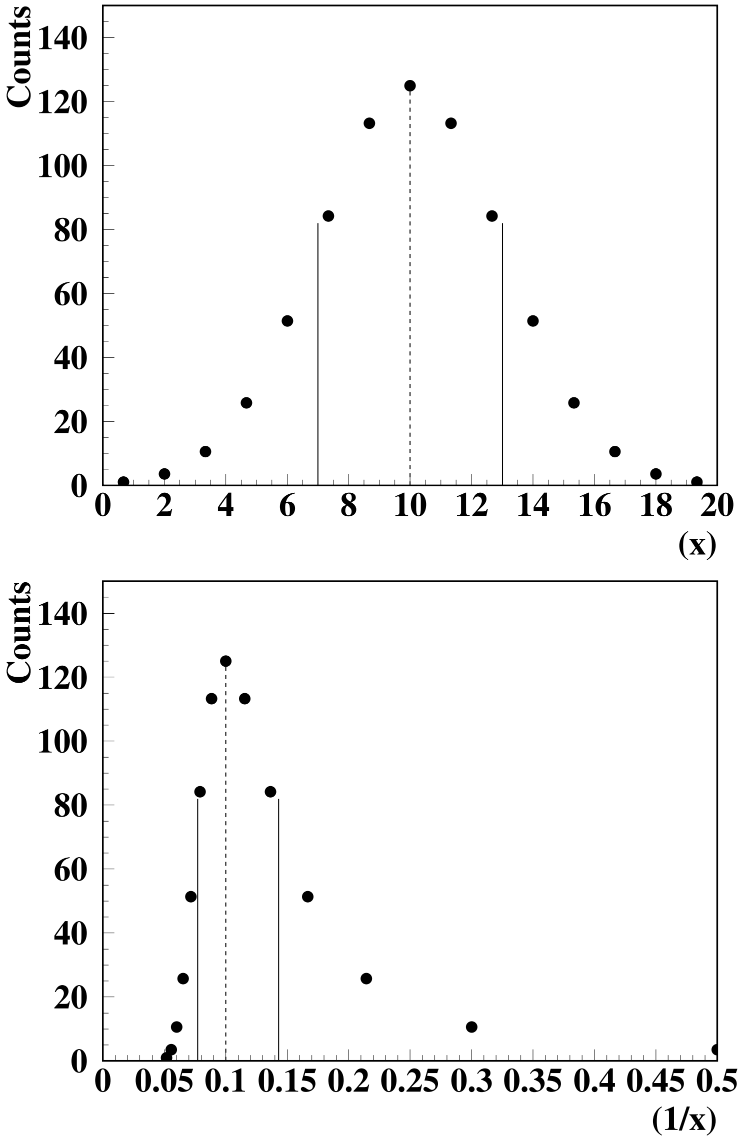

Figure D.1: (top) Gaussian distribution for x, with mean $\mu = 10$ and variance $\sigma = 3$. (bottom) Distribution of $1/x$, for the same variable x.

Almost by definition, one does not know how to combine different systematic errors. Sometimes these are combined linearly, but the general practice is to combine them in quadrature. We have followed this latter practice.

Sometimes when one is faced with assigning the total uncertainty in a result, one has the problem of combining statistical and systematic errors. Obviously, there can be no correct procedure for it. One can be very conservative and combine the two linearly or in quadrature. We have generally avoided the problem by specifying statistical and systematic errors separately. In rare cases, we have combined the two in quadrature.

3. Estimation of Errors in Fits to Data with Small Statistics

When the cross section data in the region of a resonance are fitted to a background plus a Breit-Wigner resonance, the MINUIT fit returns an estimate of the (generally) asymmetric errors. The question arises whether these errors represent the best estimate of the errors on the fit parameters. Most of the time one assumes that the Likelihood function is Gaussian. This may be a poor approximation in the case of small statistics. Thus the standard errors which are quoted by a fitting package such as MINUIT may not accurately reflect the true errors on the fit parameters. The problem becomes more acute when even the existence of the resonance is put in question. In such a case it is standard practice to quote an upper limit at a specific confidence level, for example, 90% CL. In this case, two procedures are possible.

Calculating Errors from the Likelihood Function

The first procedure is to use the results of the fit for a parameter, $\mu^{+\sigma_1}_{-\sigma_2}$, which imply a 68.27% confidence interval, $(\mu - \sigma_2, \mu + \sigma_1)$, and quote the 90% confidence upper limit as $\mu + 1.28 \times \sigma_1$. For a single free parameter, the calculation of these errors σ_1 and σ_2 by may be done as follows. With just one free parameter x, the likelihood is a function only of x. Thus $L(x)$ may be calculated for a large range of x, and integrated to determine limits and/or errors for x.

For example, the 90% confidence upper limit on x corresponds to the value $x_{90\%}$ for which the following relation holds:

$$\mathcal{A}_{90\%} = \int_{-\infty}^{x_{90\%}} L(x)dx \quad = \quad 90\% \times \int_{-\infty}^{+\infty} L(x)dx \tag{D.1}$$

This procedure does not require $L(x)$ to be Gaussian, and thus the correct upper limit $x_{90\%}$ is obtained.

The only question about this method is whether one should integrate the Likelihood function over all values of x, even if the Likelihood function has finite value in regions of x which are not physically allowed. This question is somewhat unsettled, as discussed in Ref. [108]. In both the χ_0 and η_c' analyses, in which we follow the above procedure for calculating 90% upper limits, we have tabulated both the mean value μ and the 90% upper limit so that the reader can calculate upper limits himself using a different procedure. (See Table D.1)

Estimating Errors by Monte Carlo Techniques

The other procedure is to recognize that it is incorrect to assume that the actual small statistics experiment can tell us the correct errors at all, and that one should 'repeat' the small statistics experiment a large number of times to determine the variability of the results, and assign errors and upper limits accordingly. Obviously, the large number of "repeat" experiments can be done only in Monte Carlo simulations. An example will illustrate the method.

Using the central values of best fit resonance and background parameters obtained in our analysis of the η_c data,

$$\begin{gathered}
M(\eta_c) = 2982.4^{+2.2}_{-2.4}\text{MeV} \qquad \Gamma(\eta_c) = 26.9^{+12.1}_{-8.5}\ \text{MeV} \\
B(\eta_c \to \bar{p}p) \times \Gamma(\eta_c \to \gamma\gamma) = 6.8^{+4.0}_{-2.4}\ \text{eV} \\
A_{bkg} = 12.5^{+11.41}_{-7.3}\ \text{pb} \qquad B_{bkg} = 59.0^{+39.2}_{-22.5} \\
C_{bkg} = 7.67^{+0.43}_{-0.41}\ \text{pb} \qquad D_{bkg} = 8.80^{+1.27}_{-1.58}
\end{gathered} \tag{D.2}$$

and our overall efficiency, acceptance and luminosity, we first calculated the expected number of events at each of the 146 energy points from 2911 to 3829 MeV.

We then run 10,000 Monte Carlo “experiments”. In each “experiment” we obtain a number of observed events at each E835 energy point, according to the appropriate Poisson distribution for the expected mean number of events calculated above. Each MC “experimental” spectrum is then fit for the resonance and background parameters, exactly as the experimental data was.

The distribution of the 10,000 results for the parameters $M(\eta_c)$, $\Gamma(\eta_c)$ and $B(\eta_c \to \bar{p}p) \times \Gamma(\eta_c \to \gamma\gamma)$ reflect the correct distribution functions for these parameters, from which true errors may be obtained. As an example, in Fig. D.2 we show the result of the fits for $\Gamma(\eta_c)$. From this obviously asymmetric distribution, we can obtain the positive error on $\Gamma(\eta_c)$ by integrating the distribution up from the mean value $\Gamma_0(\eta_c)$ until 68.3% of the area above the mean is covered. We obtain the negative error similarly. This procedure obtains the ±68.3% confidence interval. In the case of $\Gamma(\eta_c)$, we find that the result for the total width $\Gamma(\eta_c)$ is $26.9^{+10.8}_{-9.5}$ MeV. Note that this is different, but not substantially so, than the errors in Eq. D.2

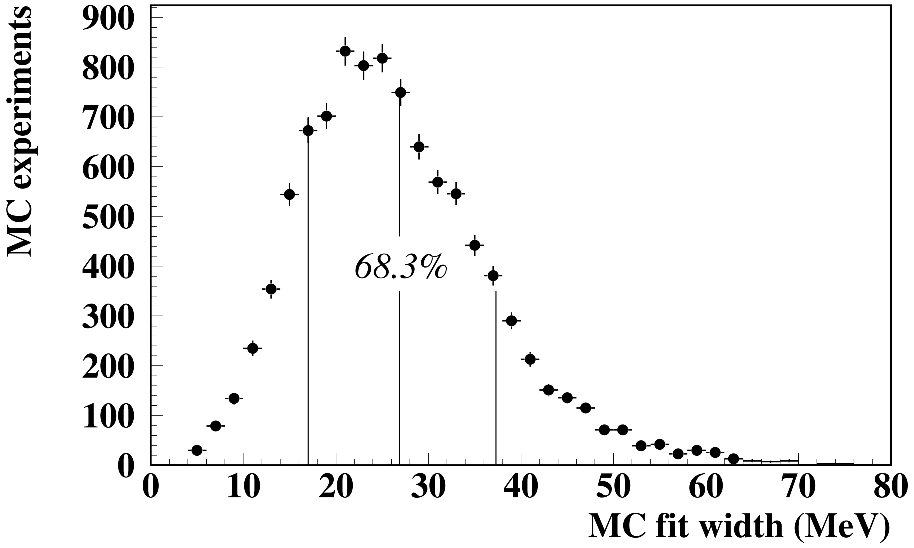

Figure D.2: Result of fits to 10,000 MC experiments for $\Gamma(\eta_c)$. The lines indicate the limits of the standard (68.3%) confidence interval. From this distribution we obtain errors on the total width of (+10.8) and (-9.5) MeV.

determined by the fit. The errors for the other resonance parameters for η_c have been obtained in a similar manner.

Table D.1: Results of fits to η_c' data. The Mass column indicates the assumed mass for the fit. The three pairs of columns indicate the mean value of $B(\eta_c'\to\bar{p}p) \times B(\eta_c'\to\gamma\gamma)$ and the 90% confidence upper limit, derived from the likelihood function.

	$\Gamma(\eta_c') = 10$ MeV		$\Gamma(\eta_c') = 15$ MeV		$\Gamma(\eta_c') = 20$ MeV	
Mass (MeV)	Mean	90% CL upper limit	Mean	90% CL upper limit	Mean	90% CL upper limit
3575	-1.2498	1.1121	-0.8510	1.2167	-0.6101	1.2283
3576	-1.0518	1.1530	-0.7324	1.2233	-0.5395	1.2188
3577	-0.8443	1.3071	-0.6192	1.2613	-0.4726	1.2220
3578	-0.6038	1.5370	-0.5129	1.3171	-0.4118	1.2342
3579	-0.3721	1.7579	-0.4218	1.3742	-0.3580	1.2509
3580	-0.2214	1.8976	-0.3550	1.4186	-0.3125	1.2682
3581	-0.1866	1.9366	-0.3168	1.4424	-0.2755	1.2840
3582	-0.2582	1.8791	-0.3039	1.4455	-0.2451	1.2977
3583	-0.3893	1.7449	-0.3061	1.4351	-0.2190	1.3107
3584	-0.5096	1.5957	-0.3098	1.4234	-0.1934	1.3254
3585	-0.5706	1.5088	-0.3027	1.4233	-0.1651	1.3444
3586	-0.5626	1.5232	-0.2777	1.4425	-0.1319	1.3694
3587	-0.4828	1.6228	-0.2337	1.4810	-0.0928	1.4011
3588	-0.3491	1.7500	-0.1759	1.5327	-0.0483	1.4388
3589	-0.2125	1.8526	-0.1119	1.5906	0.0005	1.4815
3590	-0.1140	1.9304	-0.0488	1.6507	0.0524	1.5278
3591	-0.0594	2.0074	0.0111	1.7115	0.1069	1.5770
3592	-0.0374	2.0809	0.0695	1.7723	0.1637	1.6282
3593	-0.0294	2.1220	0.1303	1.8329	0.2233	1.6810
3594	-0.0079	2.1289	0.1986	1.8948	0.2860	1.7350
3595	0.0558	2.1547	0.2785	1.9625	0.3517	1.7899
3596	0.1826	2.2591	0.3719	2.0389	0.4192	1.8449
3597	0.3770	2.4453	0.4750	2.1216	0.4873	1.8987
3598	0.6039	2.6465	0.5798	2.2025	0.5530	1.9497

Continued on next page

Results for $B(\eta_c'\to\bar{p}p) \times B(\eta_c'\to\gamma\gamma)(\times 10^8)$. *Continued from previous page*

	$\Gamma(\eta_c') = 10$ MeV		$\Gamma(\eta_c') = 15$ MeV		$\Gamma(\eta_c') = 20$ MeV	
Mass (MeV)	Mean	90% CL upper limit	Mean	90% CL upper limit	Mean	90% CL upper limit
3599	0.8038	2.7906	0.6755	2.2732	0.6141	1.9963
3600	0.9517	2.8751	0.7570	2.3286	0.6679	2.0379
3601	1.0578	2.9357	0.8182	2.3692	0.7153	2.0739
3602	1.1257	2.9761	0.8586	2.3960	0.7545	2.1057
3603	1.1361	2.9722	0.8780	2.4088	0.7871	2.1350
3604	1.0788	2.9137	0.8789	2.4113	0.8154	2.1642
3605	0.9556	2.8037	0.8665	2.4086	0.8430	2.1970
3606	0.7734	2.6473	0.8519	2.4109	0.8747	2.2376
3607	0.5699	2.4788	0.8509	2.4337	0.9170	2.2901
3608	0.4125	2.3747	0.8845	2.4957	0.9737	2.3590
3609	0.3874	2.4269	0.9734	2.6137	1.0475	2.4460
3610	0.6007	2.7228	1.1267	2.7937	1.1396	2.5489
3611	1.1072	3.2852	1.3370	3.0241	1.2434	2.6626
3612	1.7901	3.9860	1.5761	3.2779	1.3523	2.7781
3613	2.4355	4.6297	1.8113	3.5218	1.4537	2.8856
3614	2.9284	5.1260	2.0105	3.7298	1.5400	2.9745
3615	3.2730	5.5033	2.1538	3.8833	1.6006	3.0367
3616	3.4827	5.7740	2.2296	3.9674	1.6300	3.0656
3617	3.5024	5.8505	2.2275	3.9704	1.6251	3.0574
3618	3.2679	5.6294	2.1476	3.8878	1.5858	3.0116
3619	2.8327	5.1517	2.0034	3.7301	1.5159	2.9311
3620	2.3625	4.6050	1.8171	3.5208	1.4215	2.8217
3621	1.9673	4.1431	1.6100	3.2855	1.3096	2.6911
3622	1.6428	3.7689	1.4011	3.0404	1.1881	2.5468
3623	1.3356	3.4059	1.1944	2.7949	1.0622	2.3960
3624	1.0292	3.0268	0.9968	2.5545	0.9391	2.2441
3625	0.7532	2.6725	0.8134	2.3252	0.8223	2.0968
3626	0.5168	2.3698	0.6486	2.1121	0.7160	1.9586
3627	0.3039	2.0938	0.5063	1.9183	0.6234	1.8335
3628	0.1145	1.8218	0.3890	1.7476	0.5473	1.7251
3629	-0.0282	1.5752	0.3010	1.6056	0.4900	1.6369
3630	-0.1110	1.3854	0.2452	1.4987	0.4522	1.5718

Continued on next page

Results for $B(\eta_c'\to\bar{p}p) \times B(\eta_c'\to\gamma\gamma)(\times 10^8)$. *Continued from previous page*

	$\Gamma(\eta_c') = 10$ MeV		$\Gamma(\eta_c') = 15$ MeV		$\Gamma(\eta_c') = 20$ MeV	
Mass (MeV)	Mean	90% CL upper limit	Mean	90% CL upper limit	Mean	90% CL upper limit
3631	-0.1389	1.2605	0.2226	1.4324	0.4357	1.5323
3632	-0.1198	1.2005	0.2335	1.4115	0.4399	1.5201
3633	-0.0546	1.2206	0.2784	1.4406	0.4650	1.5358
3634	0.0679	1.3491	0.3593	1.5236	0.5101	1.5791
3635	0.2706	1.6144	0.4775	1.6612	0.5727	1.6474
3636	0.5762	2.0284	0.6311	1.8471	0.6495	1.7360
3637	0.9792	2.5549	0.8099	2.0642	0.7355	1.8373
3638	1.4099	3.0850	0.9946	2.2861	0.8231	1.9424
3639	1.7664	3.4962	1.1620	2.4847	0.9038	2.0424
3640	1.9960	3.7423	1.2926	2.6403	0.9725	2.1289
3641	2.1023	3.8384	1.3796	2.7448	1.0219	2.1976
3642	2.1013	3.8170	1.4203	2.8034	1.0496	2.2461
3643	2.0334	3.7376	1.4210	2.8263	1.0544	2.2741
3644	1.9528	3.6811	1.3863	2.8237	1.0354	2.2816
3645	1.8759	3.6890	1.3141	2.7974	0.9907	2.2676
3646	1.7544	3.7117	1.1955	2.7353	0.9176	2.2300
3647	1.4725	3.6051	1.0113	2.6154	0.8161	2.1650
3648	0.9064	3.1914	0.7494	2.4160	0.6842	2.0716
3649	0.0645	2.4148	0.4171	2.1341	0.5289	1.9517
3650	-0.8109	1.4823	0.0493	1.7975	0.3601	1.8139
3651	-1.4512	0.7077	-0.3000	1.4588	0.1929	1.6726
3652	-1.8522	0.2015	-0.5824	1.1724	0.0447	1.5446
3653	-2.0950	-0.0874	-0.7688	0.9751	-0.0691	1.4463
3654	-2.1601	-0.1795	-0.8505	0.8843	-0.1385	1.3898
3655	-2.0136	-0.0640	-0.8256	0.9017	-0.1595	1.3815
3656	-1.6953	0.2505	-0.7074	1.0198	-0.1341	1.4226
3657	-1.2225	0.7582	-0.5178	1.2222	-0.0686	1.5097
3658	-0.6233	1.4044	-0.2828	1.4852	0.0280	1.6370
3659	-0.0218	2.0580	-0.0303	1.7860	0.1467	1.7985
3660	0.4738	2.6421	0.2187	2.1113	0.2802	1.9897

Appendix E

Summary of All $\gamma\gamma$ Data

Table E.1: $\gamma\gamma$ candidate events, for $|\cos\theta^*| \leq 0.20$.

CM energy $\sqrt{s}$ (MeV)	Energy spread σ_E (MeV)	1st run number	N_{evt}	Luminosity $\int \mathcal{L}$ cm^{-2} sec^{-1}	Efficiency ϵ	$\sigma^{0.20}$ (pb)
2911.365	0.28610	2324	35	514.68	0.70984	95.801
2912.259	0.24760	2295	15	190.21	0.74487	105.872
2930.109	0.22000	2102	14	317.63	0.71778	61.407
2930.482	0.17010	2042	20	372.28	0.71031	75.633
2930.625	0.18170	2107	8	224.41	0.71218	50.057
2930.753	0.25560	2330	49	855.31	0.67995	84.255
2950.177	0.29460	1136	11	261.60	0.70190	59.907
2950.710	0.18510	2098	23	406.10	0.69863	81.067
2950.774	0.26960	2225	35	604.88	0.66454	87.072
2951.131	0.27060	2175	20	373.33	0.73226	73.160
2956.259	0.18000	2309	18	397.91	0.72572	62.333
2956.290	0.24020	2314	54	979.22	0.67902	81.214

Continued on next page

$\gamma\gamma$ candidate events, for $|\cos\theta^*| \leq 0.20$. *Continued from previous page*

CM energy $\sqrt{s}$ (MeV)	Energy spread σ_E (MeV)	1st run number	N_{evt}	Luminosity $\int \mathcal{L}$ cm^{-2} sec^{-1}	Efficiency ϵ	$\sigma^{0.20}$ (pb)
2966.866	0.23780	2259	30	587.86	0.68089	74.950
2966.937	0.34740	1255	15	285.76	0.70891	74.046
2970.145	0.17930	2086	22	401.54	0.72245	75.838
2973.136	0.30220	2273	45	788.67	0.68416	83.399
2973.970	0.21510	2052	41	619.80	0.68089	97.153
2975.388	0.22740	2147	14	344.59	0.68089	59.669
2980.475	0.17450	1299	30	440.73	0.72105	94.403
2980.513	0.27870	1291	13	249.94	0.70937	73.322
2983.052	0.28540	2359	66	1004.18	0.70003	93.889
2985.989	0.18930	2139	33	467.67	0.71031	99.341
2986.086	0.30270	2344	95	1410.42	0.67248	100.160
2987.575	0.27530	1271	17	341.00	0.71124	70.093
2987.749	0.19320	1093	11	249.58	0.71684	61.483
2987.998	0.22880	2188	22	370.71	0.71778	82.679
2990.660	0.24090	2162	32	499.08	0.71544	89.620
2996.140	0.20240	2065	32	742.67	0.66594	64.702
3000.857	0.25420	2155	19	347.31	0.70564	77.527
3001.308	0.21170	2184	5	209.76	0.71311	33.427
3004.917	0.31750	2298	40	1169.54	0.68649	49.821
3009.094	0.25010	2120	30	929.27	0.69863	46.209
3025.170	0.18670	1193	2	104.22	0.70704	27.142
3026.103	0.24110	1209	13	489.33	0.70050	37.926
3096.682	0.11360	3078	3	151.85	0.75841	26.050
3097.068	0.16110	824	10	274.52	0.72759	50.066
3097.137	0.14970	908	2	285.22	0.75000	9.349
3097.255	0.25810	1331	7	491.92	0.73086	19.470
3100.605	0.20100	3284	4	143.16	0.75280	37.116
3215.712	0.36110	3206	7	419.93	0.68696	24.266
3269.433	0.28740	3346	5	411.76	0.74673	16.261

Continued on next page

$\gamma\gamma$ candidate events, for $|\cos\theta^*| \leq 0.20$. *Continued from previous page*

CM energy $\sqrt{s}$ (MeV)	Energy spread σ_E (MeV)	1st run number	N_{evt}	Luminosity $\int \mathcal{L}$ cm^{-2} sec^{-1}	Efficiency ϵ	$\sigma^{0.20}$ (pb)
3318.819	0.71580	3301	6	951.38	0.68556	9.199
3405.813	0.47820	3278	2	80.67	0.66594	37.229
3406.760	0.35630	3278	13	925.95	0.66594	21.082
3414.783	0.35110	3270	7	584.95	0.62578	19.123
3414.819	0.19710	3265	3	353.18	0.71871	11.819
3418.135	0.90030	3076	2	146.25	0.73833	18.522
3418.456	0.27800	3245	2	692.03	0.69723	4.145
3429.533	0.58750	3316	3	348.75	0.74300	11.578
3429.867	0.37780	3318	2	390.24	0.76635	6.688
3494.432	0.33350	3341	5	502.79	0.67108	14.819
3508.590	0.23210	3201	3	376.23	0.64353	12.391
3509.217	0.18080	1431	0	303.97	0.71311	0.000
3509.798	0.20450	1396	0	235.09	0.71404	0.000
3509.932	0.25200	3198	0	317.08	0.65100	0.000
3510.362	0.27850	3194	2	314.95	0.63745	9.962
3510.405	0.27650	1318	4	1125.03	0.67155	5.294
3510.539	0.24610	1427	2	314.50	0.68836	9.238
3510.748	0.28990	3191	2	318.76	0.62531	10.034
3510.779	0.25750	3286	3	780.02	0.68042	5.652
3510.831	0.29490	3295	7	1147.06	0.62204	9.810
3511.053	0.30790	3188	3	319.43	0.62765	14.963
3511.172	0.21370	1394	1	218.01	0.72852	6.296
3511.445	0.31510	3185	3	315.47	0.62998	15.095
3511.752	0.20990	1424	2	319.68	0.67715	9.239
3513.002	0.30390	3181	1	301.33	0.63932	5.191
3524.642	0.30440	3081	24	3716.90	0.63092	10.234
3525.161	0.28020	3037	18	2902.98	0.64213	9.656
3525.505	0.28230	3103	16	3531.91	0.62158	7.288
3525.637	0.34600	1414	7	1800.85	0.63979	6.076

Continued on next page

$\gamma\gamma$ candidate events, for $|\cos\theta^*| \leq 0.20$. *Continued from previous page*

CM energy $\sqrt{s}$ (MeV)	Energy spread σ_E (MeV)	1st run number	N_{evt}	Luminosity $\int \mathcal{L}$ cm^{-2} sec^{-1}	Efficiency ϵ	$\sigma^{0.20}$ (pb)
3525.680	0.29210	2444	22	3477.46	0.65380	9.676
3525.782	0.28230	3060	18	2976.09	0.64306	9.405
3525.800	0.28120	3136	23	3821.46	0.61130	9.846
3525.860	0.24440	3053	9	1196.30	0.66127	11.377
3526.093	0.41110	1306	6	1985.59	0.65940	4.583
3526.105	0.29510	3005	13	2291.40	0.65333	8.684
3526.134	0.28410	1383	6	1864.73	0.64072	5.022
3526.162	0.29490	3016	18	3308.60	0.63325	8.591
3526.515	0.28170	3162	19	3233.74	0.63045	9.320
3526.520	0.31690	2404	4	975.65	0.65614	6.248
3526.610	0.29620	2439	4	649.03	0.63745	9.668
3526.841	0.38100	1403	7	1983.64	0.62625	5.635
3526.891	0.25590	2409	19	3094.13	0.63886	9.612
3527.491	0.21500	2426	10	1396.10	0.63745	11.237
3529.099	0.40230	2387	10	2328.05	0.65800	6.528
3535.451	0.53280	1244	4	1303.89	0.62718	4.891
3544.786	0.25290	774	3	997.54	0.73553	4.089
3554.655	0.37800	1379	3	489.76	0.63512	9.645
3555.164	0.28940	769	5	519.35	0.69816	13.790
3555.575	0.39120	1374	6	411.00	0.64119	22.768
3555.922	0.33010	2202	6	516.41	0.64633	17.976
3555.989	0.32990	2376	12	994.19	0.63652	18.963
3556.078	0.40830	1371	5	413.36	0.63605	19.017
3556.180	0.29520	762	2	521.27	0.69443	5.525
3556.326	0.33690	2197	7	752.35	0.61924	15.025
3556.645	0.33930	2192	13	810.30	0.62251	25.772
3556.761	0.42570	1368	5	400.58	0.64913	19.229
3557.302	0.31030	750	6	868.78	0.70237	9.833
3557.931	0.43910	1365	6	382.85	0.63979	24.495

Continued on next page

$\gamma\gamma$ candidate events, for $|\cos\theta^{*}| \leq 0.20$. *Continued from previous page*

CM energy $\sqrt{s}$ (MeV)	Energy spread σ_E (MeV)	1st run number	N_{evt}	Luminosity $\int \mathcal{L}$ cm^{-2} sec^{-1}	Efficiency ϵ	$\sigma^{0.20}$ (pb)
3555.259	0.32530	3339	4	501.02	0.66454	12.014
3556.060	0.31550	1086	7	778.22	0.74113	12.137
3576.054	0.25090	1283	8	1605.78	0.62531	7.967
3580.087	0.36050	1132	6	582.80	0.66174	15.558
3580.869	0.31880	1122	3	626.96	0.61457	7.786
3585.185	0.35770	1186	4	1505.67	0.63839	4.161
3590.246	0.35550	1112	7	1483.73	0.70424	6.699
3595.616	0.33580	1126	7	1507.36	0.65940	7.043
3600.496	0.35380	1065	10	1594.13	0.67995	9.226
3603.995	0.27080	864	10	1478.69	0.67715	9.987
3607.529	0.36130	1237	6	1523.75	0.62298	6.321
3610.583	0.41930	1036	1	922.00	0.67435	1.608
3614.707	0.31430	855	10	1538.01	0.65707	9.895
3620.586	0.35300	897	10	1471.64	0.69396	9.792
3625.299	0.30670	813	7	1637.33	0.64446	6.634
3629.747	0.36580	883	3	1618.81	0.68042	2.724
3633.144	0.35200	3309	10	2013.79	0.60803	8.167
3633.650	0.32050	3250	4	2572.89	0.60056	2.589
3635.174	0.37110	846	7	1408.19	0.64399	7.719
3639.981	0.43700	1217	10	1498.49	0.61037	10.933
3643.462	0.30400	1106	8	1233.31	0.67201	9.653
3644.296	0.36130	801	9	1723.31	0.66501	7.853
3651.632	0.28750	1199	3	1456.51	0.63792	3.229
3656.068	0.33300	1096	5	1646.01	0.62765	4.840
3660.475	0.39140	1180	6	1486.46	0.64306	6.277
3685.245	0.24330	3232	1	334.64	0.63886	4.678
3685.671	0.53980	836	7	1435.58	0.62625	7.786
3685.698	0.24560	3229	0	111.34	0.65614	0.000
3685.802	0.30740	2253	1	120.23	0.64680	12.859

Continued on next page

$\gamma\gamma$ candidate events, for $|\cos\theta^*| \leq 0.20$. *Continued from previous page*

CM energy $\sqrt{s}$ (MeV)	Energy spread σ_E (MeV)	1st run number	N_{evt}	Luminosity $\int \mathcal{L}$ cm^{-2} sec^{-1}	Efficiency ϵ	$\sigma^{0.20}$ (pb)
3685.982	0.25650	3226	1	213.12	0.63372	7.404
3686.042	0.25860	2249	0	183.15	0.65240	0.000
3686.191	0.28170	2247	0	115.73	0.64913	0.000
3686.209	0.48700	877	6	1085.27	0.67388	8.204
3686.242	0.41810	1006	2	1095.08	0.68135	2.680
3686.245	0.24860	3223	0	213.23	0.63979	0.000
3686.342	0.29320	2245	1	260.30	0.62158	6.181
3686.381	0.28140	2242	1	308.34	0.66921	4.846
3686.505	0.26310	3218	2	306.72	0.65100	10.016
3686.614	0.32350	2239	0	198.87	0.66501	0.000
3686.647	0.32030	2235	0	272.21	0.66454	0.000
3686.785	0.28140	3213	2	326.14	0.65100	9.420
3686.810	0.29310	2221	2	477.36	0.62485	6.705
3687.027	0.28560	2218	2	318.74	0.63559	9.872
3687.293	0.28820	3210	0	320.02	0.63979	0.000
3726.465	0.30210	3235	4	979.68	0.62905	6.491
3858.457	0.47220	3329	1	880.18	0.57581	1.973
4289.526	0.51810	3323	0	754.54	0.46747	0.000

Table E.2: $\gamma\gamma$ candidate events, for $|\cos\theta^*| \leq 0.40$.

CM energy $\sqrt{s}$ (MeV)	Energy spread σ_E (MeV)	1st run number	N_{evt}	Luminosity $\int \mathcal{L}$ $\mathrm{cm}^{-2}\ \mathrm{sec}^{-1}$	Efficiency ϵ	$\sigma^{0.40}$ (pb)
2911.365	0.28610	2324	225	514.68	0.72273	604.881
2912.259	0.24760	2295	92	190.21	0.76448	632.687
2930.109	0.22000	2102	106	317.63	0.73581	453.546
2930.482	0.17010	2042	132	372.28	0.73114	484.961
2930.625	0.18170	2107	79	224.41	0.73599	478.313
2930.753	0.25560	2330	261	855.31	0.70209	434.636
2950.177	0.29460	1136	87	261.60	0.71049	468.081
2950.710	0.18510	2098	128	406.10	0.72030	437.586
2950.774	0.26960	2225	189	604.88	0.68182	458.271
2951.131	0.27060	2175	119	373.33	0.74879	425.692
2956.259	0.18000	2309	119	397.91	0.73954	404.389
2956.290	0.24020	2314	281	979.22	0.69256	414.351
2966.866	0.23780	2259	170	587.86	0.70003	413.101
2966.937	0.34740	1255	88	285.76	0.71143	432.863
2970.145	0.17930	2086	120	401.54	0.73553	406.308
2973.136	0.30220	2273	226	788.67	0.70284	407.718
2973.970	0.21510	2052	170	619.80	0.69583	394.180
2975.388	0.22740	2147	81	344.59	0.69798	336.775
2980.475	0.17450	1299	116	440.73	0.72665	362.209
2980.513	0.27870	1291	81	249.94	0.72945	444.274
2983.052	0.28540	2359	290	1004.18	0.70937	407.110
2985.989	0.18930	2139	119	467.67	0.72123	352.802
2986.086	0.30270	2344	396	1410.42	0.68210	411.622
2987.575	0.27530	1271	99	341.00	0.72525	400.306
2987.749	0.19320	1093	60	249.58	0.72871	329.905

Continued on next page

$\gamma\gamma$ candidate events, for $|\cos\theta^*| \leq 0.40$. *Continued from previous page*

CM energy $\sqrt{s}$ (MeV)	Energy spread σ_E (MeV)	1st run number	N_{evt}	Luminosity $\int\mathcal{L}$ $\mathrm{cm}^{-2}\ \mathrm{sec}^{-1}$	Efficiency ϵ	$\sigma^{0.40}$ (pb)
2987.998	0.22880	2188	115	370.71	0.73020	424.836
2990.660	0.24090	2162	141	499.08	0.72450	389.949
2996.140	0.20240	2065	193	742.67	0.68854	377.424
3000.857	0.25420	2155	71	347.31	0.71871	284.437
3001.308	0.21170	2184	43	209.76	0.72292	283.568
3004.917	0.31750	2298	239	1169.54	0.70704	289.028
3009.094	0.25010	2120	195	929.27	0.71012	295.502
3025.170	0.18670	1193	27	104.22	0.71871	360.460
3026.103	0.24110	1209	78	489.33	0.71376	223.326
3096.682	0.11360	3078	13	151.85	0.77522	110.434
3097.068	0.16110	824	47	274.52	0.74412	230.082
3097.137	0.14970	908	22	285.22	0.75869	101.667
3097.255	0.25810	1331	53	491.92	0.74113	145.374
3100.605	0.20100	3284	13	143.16	0.77148	111.771
3215.712	0.36110	3206	24	419.93	0.69910	81.751
3269.433	0.28740	3346	16	411.76	0.75420	51.521
3318.819	0.71580	3301	16	951.38	0.70377	23.897
3405.813	0.47820	3278	2	80.67	0.67920	36.502
3406.760	0.35630	3278	23	925.95	0.67920	36.571
3414.783	0.35110	3270	13	584.95	0.63419	35.044
3414.819	0.19710	3265	8	353.18	0.73366	30.875
3418.135	0.90030	3076	3	146.25	0.74739	27.446
3418.456	0.27800	3245	8	692.03	0.70396	16.422
3429.533	0.58750	3316	6	348.75	0.75280	22.854
3429.867	0.37780	3318	6	390.24	0.77643	19.802
3494.432	0.33350	3341	7	502.79	0.67977	20.481
3508.590	0.23210	3201	5	376.23	0.65866	20.177
3509.217	0.18080	1431	4	303.97	0.72973	18.033
3509.798	0.20450	1396	3	235.09	0.72871	17.512

Continued on next page

$\gamma\gamma$ candidate events, for $|\cos\theta^{*}| \leq 0.40$. *Continued from previous page*

CM energy $\sqrt{s}$ (MeV)	Energy spread σ_E (MeV)	1st run number	N_{evt}	Luminosity $\int \mathcal{L}$ cm^{-2} sec^{-1}	Efficiency ϵ	$\sigma^{0.40}$ (pb)
3509.932	0.25200	3198	3	317.08	0.66109	14.312
3510.362	0.27850	3194	6	314.95	0.64605	29.488
3510.405	0.27650	1318	11	1125.03	0.68210	14.334
3510.539	0.24610	1427	3	314.50	0.70097	13.608
3510.748	0.28990	3191	3	318.76	0.63531	14.814
3510.779	0.25750	3286	9	780.02	0.69209	16.671
3510.831	0.29490	3295	17	1147.06	0.62690	23.641
3511.053	0.30790	3188	5	319.43	0.63811	24.530
3511.172	0.21370	1394	2	218.01	0.73814	12.428
3511.445	0.31510	3185	5	315.47	0.64474	24.583
3511.752	0.20990	1424	4	319.68	0.68649	18.227
3513.002	0.30390	3181	1	301.33	0.64306	5.161
3524.642	0.30440	3081	52	3716.90	0.63839	21.915
3525.161	0.28020	3037	31	2902.98	0.64353	16.594
3525.505	0.28230	3103	44	3531.91	0.63017	19.769
3525.637	0.34600	1414	24	1800.85	0.65473	20.355
3525.680	0.29210	2444	48	3477.46	0.66314	20.815
3525.782	0.28230	3060	36	2976.09	0.65025	18.603
3525.800	0.28120	3136	49	3821.46	0.62279	20.588
3525.860	0.24440	3053	20	1196.30	0.66781	25.034
3526.093	0.41110	1306	18	1985.59	0.66706	13.590
3526.105	0.29510	3005	36	2291.40	0.65800	23.877
3526.134	0.28410	1383	20	1864.73	0.65399	16.400
3526.162	0.29490	3016	41	3308.60	0.64371	19.251
3526.515	0.28170	3162	41	3233.74	0.63671	19.913
3526.520	0.31690	2404	12	975.65	0.65912	18.660
3526.610	0.29620	2439	10	649.03	0.64371	23.936
3526.841	0.38100	1403	18	1983.64	0.64306	14.111
3526.891	0.25590	2409	36	3094.13	0.64558	18.022

Continued on next page

$\gamma\gamma$ candidate events, for $|\cos\theta^{*}| \leq 0.40$. *Continued from previous page*

CM energy $\sqrt{s}$ (MeV)	Energy spread σ_E (MeV)	1st run number	N_{evt}	Luminosity $\int\mathcal{L}$ cm^{-2} sec^{-1}	Efficiency ϵ	$\sigma^{0.40}$ (pb)
3527.491	0.21500	2426	16	1396.10	0.66267	17.294
3529.099	0.40230	2387	28	2328.05	0.67061	17.935
3535.451	0.53280	1244	12	1303.89	0.63587	14.474
3544.786	0.25290	774	8	997.54	0.73814	10.865
3554.655	0.37800	1379	9	489.76	0.64698	28.403
3555.164	0.28940	769	12	519.35	0.70657	32.701
3555.575	0.39120	1374	9	411.00	0.64558	33.920
3555.922	0.33010	2202	12	516.41	0.65315	35.578
3555.989	0.32990	2376	26	994.19	0.64521	40.533
3556.078	0.40830	1371	10	413.36	0.64539	37.484
3556.180	0.29520	762	11	521.27	0.69676	30.286
3556.326	0.33690	2197	14	752.35	0.63260	29.416
3556.645	0.33930	2192	24	810.30	0.63092	46.945
3556.761	0.42570	1368	10	400.58	0.65735	37.976
3557.302	0.31030	750	14	868.78	0.70638	22.813
3557.931	0.43910	1365	8	382.85	0.64941	32.177
3555.259	0.32530	3339	12	501.02	0.66828	35.840
3556.060	0.31550	1086	22	778.22	0.74954	37.716
3576.054	0.25090	1283	13	1605.78	0.63447	12.760
3580.087	0.36050	1132	9	582.80	0.67014	23.044
3580.869	0.31880	1122	7	626.96	0.61906	18.036
3585.185	0.35770	1186	13	1505.67	0.64521	13.382
3590.246	0.35550	1112	18	1483.73	0.70610	17.181
3595.616	0.33580	1126	14	1507.36	0.65754	14.125
3600.496	0.35380	1065	20	1594.13	0.68883	18.214
3603.995	0.27080	864	21	1478.69	0.68649	20.687
3607.529	0.36130	1237	14	1523.75	0.63484	14.473
3610.583	0.41930	1036	2	922.00	0.68089	3.186
3614.707	0.31430	855	31	1538.01	0.66127	30.481

Continued on next page

$\gamma\gamma$ candidate events, for $|\cos\theta^*| \leq 0.40$. *Continued from previous page*

CM energy $\sqrt{s}$ (MeV)	Energy spread σ_E (MeV)	1st run number	N_{evt}	Luminosity $\int \mathcal{L}$ cm^{-2} sec^{-1}	Efficiency ϵ	$\sigma^{0.40}$ (pb)
3620.586	0.35300	897	18	1471.64	0.69863	17.507
3625.299	0.30670	813	17	1637.33	0.65380	15.881
3629.747	0.36580	883	15	1618.81	0.68714	13.485
3633.144	0.35200	3309	22	2013.79	0.60850	17.953
3633.650	0.32050	3250	13	2572.89	0.60757	8.316
3635.174	0.37110	846	18	1408.19	0.65165	19.615
3639.981	0.43700	1217	20	1498.49	0.61709	21.628
3643.462	0.30400	1106	20	1233.31	0.68341	23.729
3644.296	0.36130	801	23	1723.31	0.66921	19.943
3651.632	0.28750	1199	8	1456.51	0.64119	8.566
3656.068	0.33300	1096	8	1646.01	0.63699	7.630
3660.475	0.39140	1180	20	1486.46	0.64773	20.772
3685.245	0.24330	3232	1	334.64	0.65287	4.577
3685.671	0.53980	836	15	1435.58	0.62858	16.623
3685.698	0.24560	3229	1	111.34	0.66594	13.487
3685.802	0.30740	2253	1	120.23	0.66193	12.565
3685.982	0.25650	3226	1	213.12	0.64287	7.299
3686.042	0.25860	2249	3	183.15	0.66155	24.760
3686.191	0.28170	2247	0	115.73	0.66407	0.000
3686.209	0.48700	877	20	1085.27	0.68509	26.900
3686.242	0.41810	1006	5	1095.08	0.68901	6.627
3686.245	0.24860	3223	1	213.23	0.64698	7.249
3686.342	0.29320	2245	2	260.30	0.63512	12.098
3686.381	0.28140	2242	6	308.34	0.67790	28.705
3686.505	0.26310	3218	3	306.72	0.65847	14.854
3686.614	0.32350	2239	2	198.87	0.67949	14.801
3686.647	0.32030	2235	5	272.21	0.67360	27.269
3686.785	0.28140	3213	5	326.14	0.65847	23.283
3686.810	0.29310	2221	6	477.36	0.64166	19.589

Continued on next page

$\gamma\gamma$ candidate events, for $\lvert\cos\theta^*\rvert \leq 0.40$.	*Continued from previous page*					
CM energy $\sqrt{s}$ (MeV)	Energy spread σ_E (MeV)	1st run number	N_{evt}	Luminosity $\int\mathcal{L}$ cm^{-2} sec^{-1}	Efficiency ϵ	$\sigma^{0.40}$ (pb)
3687.027	0.28560	2218	2	318.74	0.64184	9.776
3687.293	0.28820	3210	0	320.02	0.63811	0.000
3726.465	0.30210	3235	9	979.68	0.63811	14.397
3858.457	0.47220	3329	1	880.18	0.58347	1.947
4289.526	0.51810	3323	0	754.54	0.46915	0.000